Plasticity of the adult human small intestinal stoma microbiota

Yilmaz, Bahtiyar; Fuhrer, Tobias; Morgenthaler, Deborah; Krupka, Niklas; Wang, Daoming; Spari, Daniel; Candinas, Daniel; Misselwitz, Benjamin; Beldi, Guido; Sauer, Uwe

Published in:
Cell Host and Microbe

DOI:
10.1016/j.chom.2022.10.002

Publication date:
2022

Cell Host & Microbe

CellPress

Resource

Plasticity of the adult human small intestinal stoma microbiota

Bahtiyar Yilmaz,[1,2,3,*] Tobias Fuhrer,[4] Deborah Morgenthaler,[1,2] Niklas Krupka,[1,2] Daoming Wang,[5,6] Daniel Spari,[1,2] Daniel Candinas,[1,2] Benjamin Misselwitz,[1,2] Guido Beldi,[1,2] Uwe Sauer,[4] and Andrew J. Macpherson[1,2,3,7,*]

[1]Department of Visceral Surgery and Medicine, Bern University Hospital, University of Bern, 3010 Bern, Switzerland
[2]Maurice Müller Laboratories, Department for Biomedical Research, University of Bern, 3008 Bern, Switzerland
[3]Bern Center for Precision Medicine (BCPM), University of Bern, 3008 Bern, Switzerland
[4]Institute of Molecular Systems Biology, Swiss Federal Institute of Technology (ETH) Zürich, 8093 Zürich, Switzerland
[5]Department of Genetics, University of Groningen, University Medical Center Groningen, Groningen 9713AV, the Netherlands
[6]Department of Pediatrics, University of Groningen, University Medical Center Groningen, Groningen 9713AV, the Netherlands
[7]Lead contact
*Correspondence: bahtiyar.yilmaz@dbmr.unibe.ch (B.Y.), andrew.macpherson@dbmr.unibe.ch (A.J.M.)
https://doi.org/10.1016/j.chom.2022.10.002

SUMMARY

The human distal small intestine (ileum) has a distinct microbiota, but human studies investigating its composition and function have been limited by the inaccessibility of the ileum without purging and/or deep intubation. We investigated inherent instability, temporal dynamics, and the contribution of fed and fasted states using stoma samples from cured colorectal cancer patients as a non-invasive access route to the otherwise inaccessible small and large intestines. Sequential sampling of the ileum before and after stoma formation indicated that ileostoma microbiotas represented that of the intact small intestine. Ileal and colonic stoma microbiotas were confirmed as distinct, and two types of instability in ileal host-microbial relationships were observed: inter-digestive purging followed by the rapid postprandial blooming of bacterial biomass and sub-strain appearance and disappearance within individual taxa after feeding. In contrast to the relative stability of colonic microbiota, the human small intestinal microbiota biomass and its sub-strain composition can be highly dynamic.

INTRODUCTION

Stool microbiota analyses have been extensively correlated with many different metrics of health and disease, although microbiota composition is considered relatively stable within healthy individuals after successive waves of colonization in the early life (Bäckhed et al., 2015; Faith et al., 2013; Garud et al., 2019; Lou et al., 2021; Olm et al., 2021; Zhao et al., 2019). Beyond correlations, we generally lack sufficient understanding of causalities and mechanisms by which microbes might influence the host status. Rodent studies are starting to fill this gap by using germ-free and genetically targeted animals to define mechanisms of host-microbial mutualism. Animal models are limited by fundamental differences between species; for example, rodents re-inoculate their proximal intestine through coprophagy and have a far shorter large intestinal transit time (~6 h in mice and >24 h in humans) (Miller et al., 1997; Padmanabhan et al., 2013; Proano et al., 1990). Although humans generally avoid microbial contamination of their diet or fluid intake, they nevertheless have a distinct microbiota in the distal small intestine (terminal ileum) with an increased proportion of aerobes compared with the colon (Finegold et al., 1970; Gorbach et al., 1967). The biomass of the healthy ileal microbiota is substantially less than that of the colon (Hill and Marsh, 1989), but it can shape the epithelial gene expression (Hooper et al., 2001), intestinal physiology (Stappenbeck et al., 2002), nutrition, and molecular exchanges between the microbes and their host (Holmes et al., 2011). Disturbances of human small intestinal microbiota occur in patients with motility disorders or surgically created blind loops when an overgrowth of small intestinal microbes causes abdominal pain and malabsorption, with vitamin B12 depletion and bile salt deconjugation (Drasar and Shiner, 1969). Unfortunately, human terminal ileum is inaccessible without surgery, very extensive peroral/nasal intubation, or purging prior to colonoscopy (Hill, 2020): this has limited investigation of the characteristics and dynamics of its specific microbiota as individuals transition between digestive and inter-digestive phases.

One alternative to access human intestine without invasive procedures or prior purging involves subjects who have had disconnection of intestinal continuity at surgery, which creates an opening (stoma) of the bowel through the anterior abdominal wall. This is a standard life-saving procedure in visceral surgery, which allows the bowel to recover from events such as surgical removal of diseased intestinal segments, inflammation, infection, or stab wounds (Martin and Vogel, 2012). Depending on the condition being treated, such as colorectal cancer (CRC) or

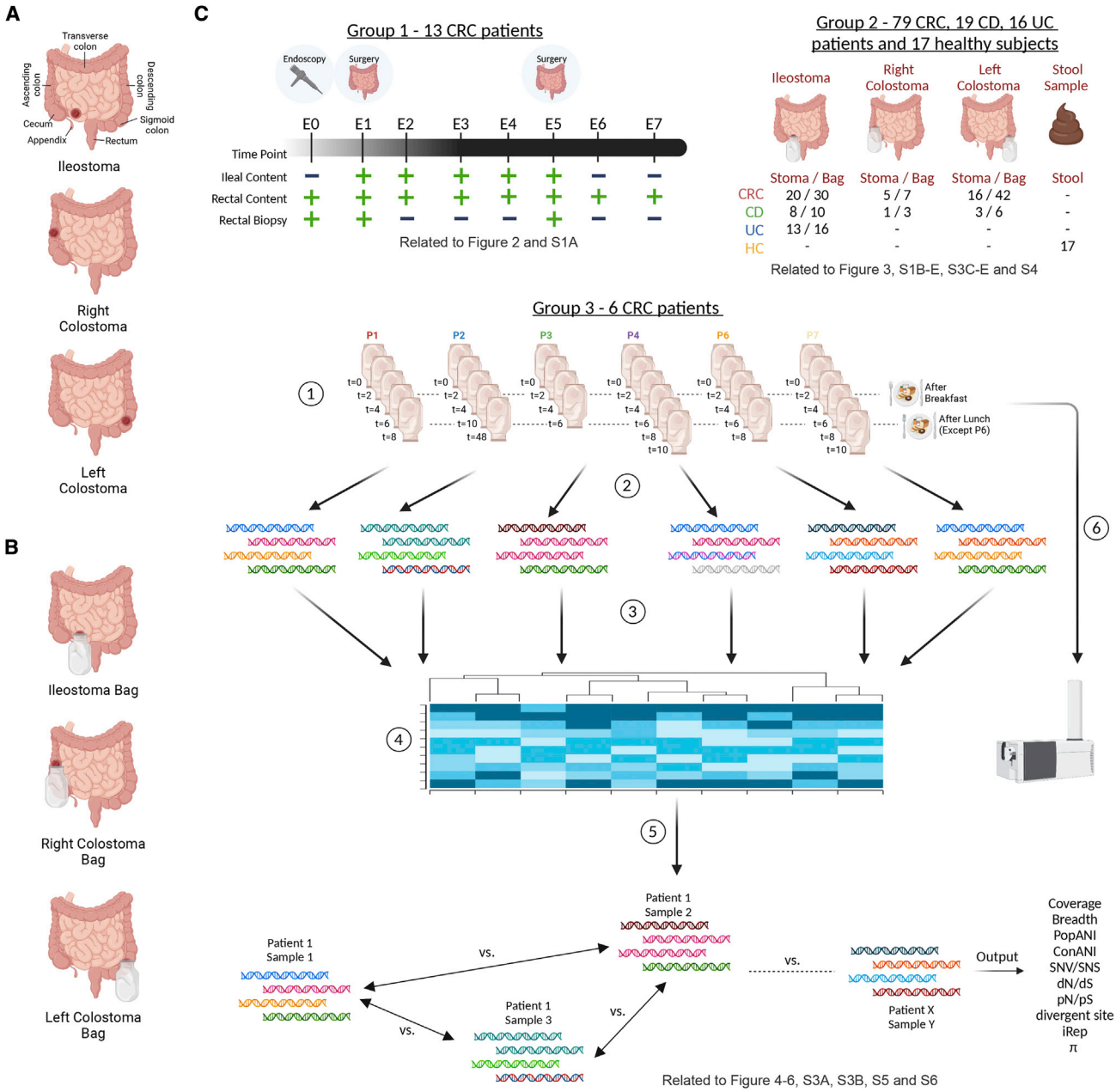

Figure 1. Overview of study cohorts and metagenomic inStrain pipeline

(A) Diagram showing an ileostomy and two types of colostomies (right in the ascending colon and left in the sigmoid colon).

(B) Diagram showing a stoma bag attached to ileostoma or two types of colostomas.

(C) Study groups: group 1 comprises CRC patients who underwent surgery. Ileal and rectal biopsy and luminal samples were collected directly before, during, and after surgery over 6–12 months. Group 2 comprises CRC, CD, UC patients with a stable stoma and healthy controls (HCs). The number of patients were reported as stoma/bag; group 3 comprises CRC patients. Serial samples from stoma were collected before and after they had eaten a standardized diet provided by hospital catering for the next 10–48 h (1). Samples were subjected to shotgun sequencing (2), and reads were mapped to reference databases (3) for sample-specific relative abundance calculation (4) and processed in the inStrain pipeline - (5) for coverage, breadth, ANI, PopANI, SNVs, dN/dS, pN/pS, and nucleotide diversity and in untargeted metabolomics (6). Figure created with BioRender.com.

inflammatory bowel diseases (IBDs), the stoma may be at the level of the distal small intestine (ileostomy) or sited proximally or distally along the large intestine (colostomy) (Figures 1A and 1B). The disruption of intestinal continuity inevitably causes some physiological adaptation, which can be minimized by limiting the amount of small intestine that is surgically removed when the stoma is fashioned (Cooper et al., 1986). Many patients have been cured of their original condition and remain stable over many years with an otherwise normal diet and lifestyle: their ileostomas allow non-invasive sequential sampling without

oropharyngeal contamination of catheters, purging for endoscopy, or limitations of concurrent surgery in diseased patients (Finegold et al., 1983). Small intestinal flow rates are not increased in patients with ileal stomas (Ladas et al., 1986).

Studies on stoma patients have been especially valuable in investigating human digestive processes and the microbial consortia in different intestinal segments. Ileal microbiota profiles depend on the capacity for rapid import and utilization of relatively simple carbohydrates with rapid adaptation to nutrient availability, whereas the colonic microbiota is mostly specialized in the efficient degradation of complex carbohydrates (Zoetendal et al., 2012). Ileostomy fluids have been shown to contain dietary fiber and complex carbohydrates resistant to human digestion, especially from plant cell walls (Englyst and Cummings, 1987; Florin et al., 1990; Macfarlane and Englyst, 1986; Silvester et al., 1995; van Trijp et al., 2020) that are normally harvested through colonic microbial fermentation (Pomare et al., 1985). A minor but significant fraction of dietary fibers and oligogalactose/oligofructan can be degraded by the small intestinal microbiota. Higher molecular weight fibers inulin, lemon pectin, and iso-malto/maltopolysaccharides are fermented at a slower rate in the small intestine with a subject-dependent response (Livesey et al., 1995; Sundberg et al., 1996; van Trijp et al., 2020).

Stoma studies have also distinguished the roles of different human intestinal segments in nitrogen and sulfur balance and sites of uptake of different molecular substrates (Duffy et al., 2002; Florin et al., 1990). Ileostomas have also been used to map the microbial composition of the distal small intestine and to determine the recovery of intestinal function and the ileal microbiota following intestinal transplantation (Hartman et al., 2009). In limited numbers of subjects, the ileal microbiota has been shown to correlate with the microbiota in ileal stoma effluents (Ahmed et al., 2007; Stolaki et al., 2019; Zoetendal et al., 2012)

Our hypothesis was that the human small intestinal microbiota biomass and its strain composition would be very dynamic over the feed-fast cycle compared with the relatively stable colonic microbiota (Faith et al., 2013). Using ileal and colonic stoma patients for real-time access, we show here that there is an inherent instability in the human small intestinal microbiota biomass relating to dietary pulsations within individuals. Despite these rapid small intestinal transit and large biomass fluctuations, we find that the composition at the taxon level of the small intestinal microbiota remains relatively stable. This apparent stability conceals rapid dynamic fluctuations of bacterial sub-strains within individual taxa, some of which bloom within hours from undetectable levels, indicating that even after inter-digestive purging of small intestinal microbes, sufficient diversity of microbial strains and sub-strains persists to reconstitute the microbiota, allowing adaptation potential within individual taxa as conditions change within the intestinal lumen.

RESULTS

Validation of stoma samples as representing the natural small intestinal microbiota

The validity of microbial ileostoma studies depends on how closely they model the natural situation of the fully connected intestine. We therefore started by asking how far surgical manipulations or intestinal discontinuity disrupt the microbial communities in the distal small intestine. To address this, we carried out a longitudinal study where ileal and rectal samples were collected directly at surgery, followed by sequential sampling at 1–2 monthly intervals from the same patient's ileal stoma site over the next 6–12 months (Figures 1C and 2; Table S1). Samples from each patient and at least 3 follow-up samples were processed and analyzed using the 16S IonTorrent sequencing technology for microbial composition (>5,000 reads/sample). Alpha diversities of ileal samples showed fluctuations, but there were no significant differences over time in either alpha (Figure 2A) or beta diversities (Figure 2B). A control situation in these patients without needing to carry out further clinical manipulations was to follow the microbiota of the remaining colon in ileostomy patients left *in situ* as a separated mucous fistula. Here, we would expect a microbiota composition change, as it had been disconnected from its regular carbon source intake of undigested material from the small intestine. In some cases, this can result in inflammation of the isolated colonic segment because of deprivation of microbiota-derived short-chain fatty acids. As expected, beta diversities of the rectal samples from the disconnected colon changed after surgery, and microbiota composition continued to be shaped over time (Figure 2B).

Analysis of specific changes of individual taxa over time from both sets of samples was carried out (Figures 2C and 2D; Table S2). No taxon in the ileal samples retained significance after Benjamini-Hochberg adjustment for multiple testing (Figure 2C). Specifically, the *Enterobacteriaceae* family underwent personalized fluctuations, with some patients showing a bloom immediately after surgery, but there were no significant differences between the sequential samples (Figure S1A). In contrast, in rectal samples from the excluded colon *Lachnoclostrium* and *Dialister* significantly increased, and *Faecalibacterium*, *Ruminococcaceae*, *Barnesiella*, *Butyricimonas*, and *Subdoligranulum* decreased over time (Figure 2D). Given our positive controls of microbiota alterations in the disconnected colon, we concluded that despite considerable interpersonal differences and fluctuations in ileal samples after stoma formation, there were no overall significant differences compared with the original ileal sample taken before disrupting intestinal continuity by surgery.

The distinct diversity of ileostoma microbiota according to age, disease status, or exposure parameters

We next asked whether we could identify relationships affecting distal intestinal microbiota diversity based on factors of age, gender, body habitus, smoking exposures, or use of antibiotics within the last 3 months. Although dietary data were collected, there were insufficient differences between subjects for meaningful analysis. We investigated 141 stoma samples of 79 patients who had recovered from surgery for distal colonic cancers (CRC: 38% ileostomy, 10% right-sided colonic stomas, and 52% left-sided colonic stomas: Figure 1C; Table S1). These patients were selected after recovery from their original condition to be as close as possible to healthy subjects despite their stoma. Luminal contents were taken from the stoma or bag during a morning appointment 2–4 h after breakfast and analyzed for microbial composition. The results showed lower alpha diversity in ileum compared with left colonic stomas of CRC patients or

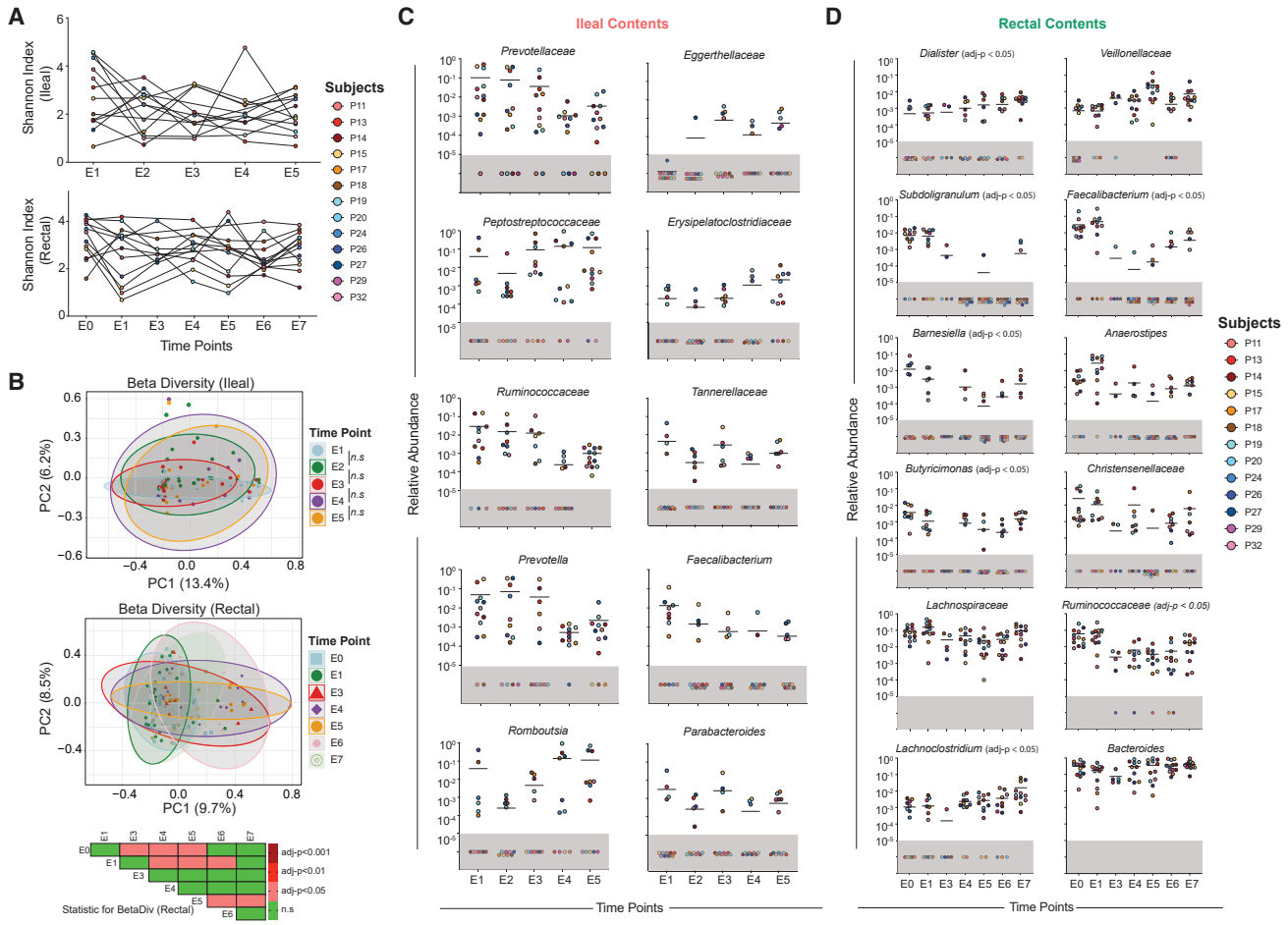

Figure 2. Microbiota compositions in the ileum or rectum at different times after surgery

(A) Longitudinal microbial richness is shown in the ileum and rectum in 13 CRC patients who underwent surgery. Significant differences between groups were tested by linear mixed models, and patient ID and smoking status were included as a random effect. *E0: before surgery (1st visit session), E1: surgery (2nd visit session), E2–E7: after surgery (3rd–8th visit session).* See also Table S1.

(B) Microbial clustering for ileum (upper panel) and rectum (lower panel) over time is shown based on Bray-Curtis dissimilarity PCoA plots. The ellipse colors show clustering of each time point with 95% confidence intervals (q values as in the heatmap, n.s. non-significant).

(C and D) Microbial taxa changes over time in the ileum (C) and rectum (D) are shown based on relative abundances. Gray shading shows taxa values below detection limits and mean values are shown. Patient samples vary according to individual attendance at each time point.

(C) E1–E3 contains samples from 15 patients; E4 contains samples from 9 patients, and E5 contains samples from 13 patients.

(D) E0 contains samples from 13 patients; E1, E5, E6, and E7 contain samples from 12 patients; E3 contains samples from 5 patients; and E4 contains samples from 11 patients. Each color represents a patient. $q < 0.05$ was considered significant. Taxa were selected based on the lowest non-adjusted p values: unless shown, q values were non-significant.

See also Figure S1.

healthy fecal samples (Figure 3A). There were distinct beta diversities of the ileal samples compared with either the right colon or left colon, or between right and left colon sites, in CRC patients ($p < 0.05$) (Figure 3B). In contrast, we did not observe any significant differences in the microbiota or metabolomic profiles from stoma effluents collected directly from the bag or by cannulating the stoma (Figures S1B–S1D).

Most taxa of the *Enterobacteriaceae* and the Bacilli class of the Firmicutes were generally enriched in the ileum, in line with facultative anerobic metabolism. In contrast, anerobic *Bacteroidaceae*, *Prevotellaceae*, *Lachnospiraceae*, and *Ruminococcaceae* families dominated in the colon (Figures 3C and 3D; Table S2). We found that small intestinal contents contained a relatively higher abundance of *Lactobacillus*, *Clostridium*, *Streptococcus*, *Enterococcus*, and *Veillonella*, and a lower abundance of *[Ruminococcus]* and *Bacteroides*. Exceptions to these general patterns were found in divisions with taxa enriched in the proximal colon (*Bilophila* and *Desulfovibrio* of the *Deltaproteobacteria*), and Bacteroidetes and *Ruminococcaceae* were mostly enriched in the left (distal) colon (Figures 3C and 3D; Table S2). These phylogenetic distributions are aligned with previous studies of the biogeography of the normal human intestine (Bentley et al., 1972; Booijink et al., 2010; Donaldson et al., 2016), supporting the validity of using ileostoma patients to investigate the dynamics of intestinal microbiota at different locations of the intestinal tract.

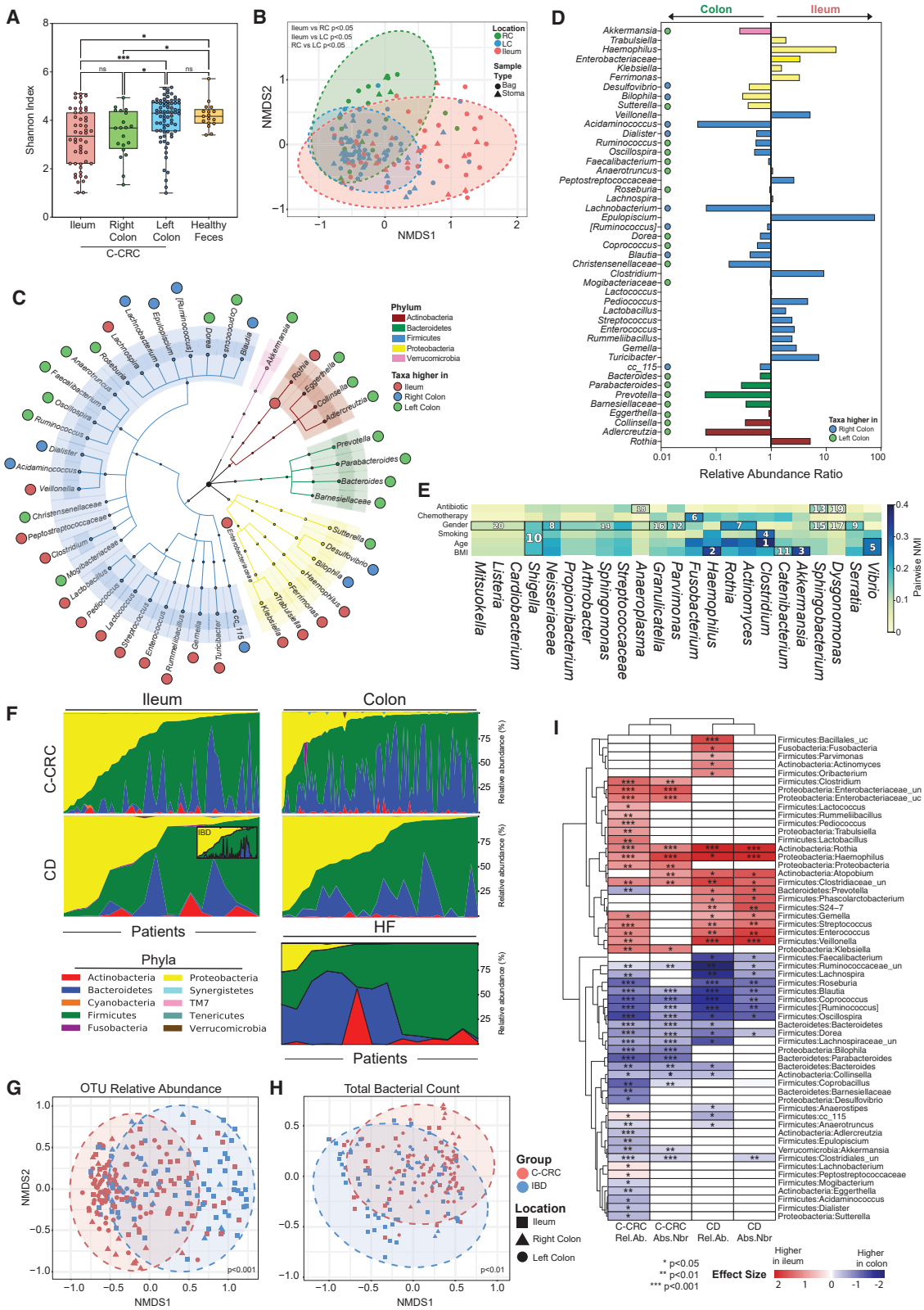

(legend on next page)

We did find differences in the small intestinal microbiota of cured CRC patients according to the age of the patient (*Clostridia*), BMI (body mass index; Proteobacteria and Verrucomicrobia), and smoking (Proteobacteria and *Clostridia*) with only weak effects according to gender or the use of antibiotics in the last 3 months (Figure 3E). Crohn's disease (CD) patients had an altered microbiota profile in the small and large intestines. (Surgical treatment of ulcerative colitis [UC] form of IBD requires a total colectomy; hence, colonic stomas are not usually available for study.) Although alpha diversity overall did not differ between cured CRC and IBD patients sampled at different stoma sites (Figure S1E), Proteobacteria that were enriched in the ileum of cured CRC patients had an even distribution between CD ileum and colon stomas assessed either by relative abundance or absolute biomass quantification (Figures 3F–3I; Table S2). There is therefore evidence that small intestinal microbiota is influenced by BMI and age, as well as disruption of the spatial distribution of the microbiota in intestinal inflammatory disease.

Expansion of the microbial biomass between fasting and feeding in the distal small intestine

Having verified that microbiota of ileostomas is representative of the natural human small intestine, we next exploited the non-invasive access route to make sequential measurements of how the ileal microbiota varies within each individual from the fasting to the fed state.

We took serial samples following consumption of a standardized breakfast over 6–48 h from ileal stomas in the second group of 6 cured CRC patients who had fasted overnight (Figures 1C and 4). Shotgun metagenomic sequencing datasets were analyzed using metagenomic intra-species diversity analysis system (MIDAS) (Nayfach et al., 2016) and inStrain (Olm et al., 2021) pipelines. Metagenomic sequences from stoma contents overall showed equivalent metagenomic reads of bacteria and host DNA with smaller read numbers of archaea and viruses (Figure 4A). However, before the test, meal samples mostly consisted of human host DNA in line with shedding small intestinal epithelial cells into the intestine during the overnight fast (Figure 4B). Following the meal, patients had a significant increase in recovered microbial sequences (Figure 4B) manifested by increased overall (prokaryotic + eukaryotic) alpha diversity (Figure 4C main). If we excluded human host sequences from the analysis, there was no significant change in bacterial or archaeal alpha diversity after eating (Figure 4C inset; Figure S2A). However, early 2-h postprandial blooms of Proteobacteria were compensated by corresponding proportional reductions in Firmicutes (Figures S2B–S2D). It is well established that gastrointestinal blood flow and oxygen delivery to the intestine increase after meals (Madsen et al., 2006), consistent with a bloom of Proteobacteria over anerobic Bacteroidetes and Clostridia (Byndloss et al., 2017). Since the extraction protocol used was optimized for DNA, RNA viruses were not sequenced. However, low numbers of recovered DNA viral sequences were also obtained, but the inferred viral diversity (dominated by *Polydnaviridae*, *Myoviridae*, and *Siphoviridae*) did not change after feeding (Figure S2E).

The proportion of microbial sequences dropped again after 4 or 6 h, apart from one patient (P6), with a slow continuous rise from 2 to 8 h (Figure 4B). Further rises in recovered proportions of microbial DNA occurred at or after 6 h following a second meal. Variable orocecal transit times are due to differences in gastric emptying and the composition of the test substances used for their measurement: median values between 53 and 204 min are found using different techniques (Miller et al., 1997).

We concluded that there was increased biomass of the distal small intestinal microbiota after feeding, which contracted again after the wave of dietary nutrients had passed. We confirmed directly that this postprandial effect on the distal small intestinal microbiota corresponds to an increased ileal microbial biomass after an overnight fast in 4 independent ileostoma patients by quantitative bacterial flow cytometry, which showed 10-fold increases in absolute numbers of microbes after 2 and 4 h

Figure 3. Distinct microbial features associated with CRC and IBD stoma patients

(A) Microbial richness differences at different sites of the disconnected intestine in CRC patients' stomas and healthy subjects' feces are plotted using the Shannon index. Significant differences between groups were determined by an ordinary one-way ANOVA corrected for multiple comparisons using Benjamini and Hochberg false discovery rate (BH-FDR) and $q < 0.05$ was considered significant.

(B) Microbial clustering based on Bray-Curtis dissimilarity. Ellipse coloring shows clusters of intestinal locations at 95% confidence intervals. Non-parametric analysis of variance (Adonis) was used to test significant differences between anatomic locations: $p < 0.05$ was considered significant.

(C and D) Overall representation of significant taxa according to stoma locations in cured CRC patients is shown using phylogenetic trees (C) and as relative abundance ratios on a bar plot (D). Red, blue, and green circles represent higher relative abundances in ileum, right colon, and left colon, respectively. $q < 0.2$ ($p < 0.05$) was considered significant.

(E) Hierarchical analysis performed using end-to-end statistical method (HAllA) at the genus level. Correlating clinical metadata was plotted after BH-FDR correction: $q < 0.2$ (and $p < 0.05$) was considered significant (A–D). Association rank was sorted by high similarity score. The color intensity of the heatmap (pairwise normalized mutual information [NMI]) and numbers in cells identify significant pairs of features (clinical determinants versus microbial composition) of ileostomy CRC patients.

(F) Overall taxonomy representation of CRC and CD patients and healthy control feces (HF) stratified according to ascending Firmicutes/Proteobacteria ratio. Inset, ileum of IBD patients.

(G and H) Microbial clustering based on Bray-Curtis dissimilarity of different intestinal sites from CRC and CD patients using (G) relative abundance or (H) total bacterial mass. Ellipse colors show clustering of disease groups with 95% confidence intervals.

(I) Taxa significantly associated with ileum or colon of CRC or CD groups are shown based on relative abundance and total bacterial mass information. The higher relative abundance of a taxon in the ileum or colon is shown in red or blue, respectively. Differential abundance was assessed using *MaAsLin2* with the BH-FDR approach; $q < 0.2$ ($p < 0.05$) was considered significant as in (D). Unclassified genera are denoted *_uc*, classified but unnamed genus *_un*. Asterisks for p values: $^{*}p < 0.05$, $^{**}p < 0.01$, and $^{***}p < 0.001$. (A)–(G) and (I) contain 50 ileum samples, 20 right colon samples, 71 left colon samples from CRC patients, and 17 healthy feces. (F) contains 65 ileum samples and 30 colon samples from IBD patients. (H) and (I) contain 30 ileum samples, 15 right colon samples, 52 left colon samples from CRC patients, and 53 ileum samples, 18 right colon samples, and 8 left colon samples from IBD patients.

See also Figures S3 and S4.

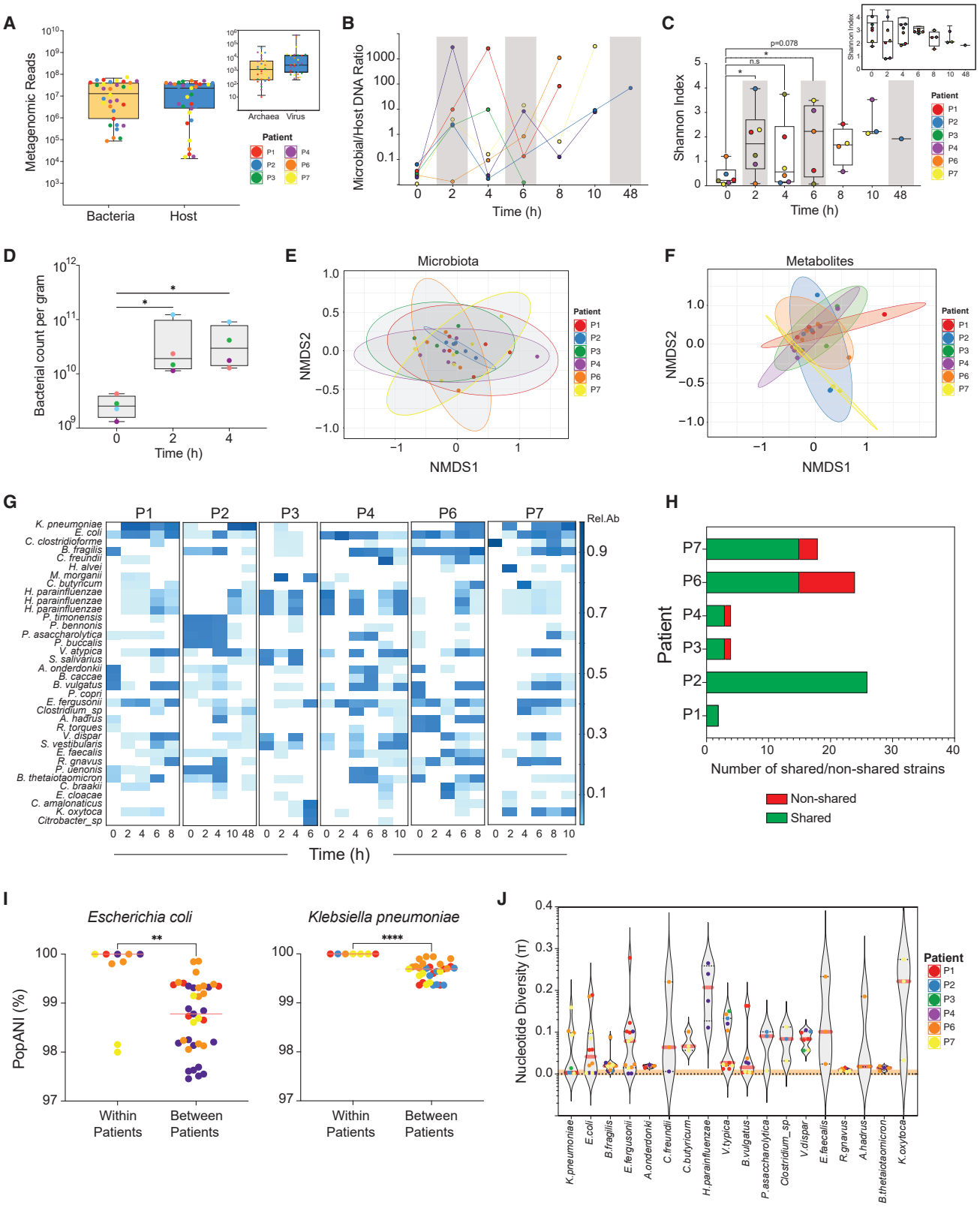

(legend on next page)

following breakfast (Figure 4D). Although these results are from ileostoma patients, measurements during nasoileal intubation show that ileostoma fluid flux is no faster than in healthy controls (HCs) with an intact intestine (Ladas et al., 1986), suggesting that the inter-digestive microbial load purging from the small intestine is likely also true of normal subjects.

Changes in available ileal carbon sources and other metabolites following a meal

The kinetics of the large postprandial bloom in the distal small intestinal microbiota indicated that in most subjects, the available carbon sources for bacterial growth and division start to reach the ileum 2 h after a meal and are entirely purged after a 12 h fast at the latest. Previous work has shown that these carbon sources include fiber and starch polymers that are resistant to human glycoside hydrolases in the proximal small intestine (Pomare et al., 1985; Silvester et al., 1995). We therefore asked whether the overall chemical environment of the distal small intestine also undergoes large postprandial transitions, matching those of the microbiota biomass and the delivery of undigestible polymers from the diet or whether the luminal organic environment is buffered by proximal host digestion and consumption by the ileal microbiota of residual simple carbon sources.

To achieve the required breadth and depth of molecular discrimination of intestinal contents, we employed high-resolution untargeted mass-spectrometry on the ileostoma contents with a high-throughput methodology (Fuhrer et al., 2011, 2017; Sévin et al., 2017). This could potentially resolve over 1,000 compounds ranging from 50 to 1,000 Da annotated to metabolite ions based on accurate mass with 1-mD tolerance, which allowed us to capture the spectrum of luminal organic compounds independently of undigested fiber or other high polymers (Fuhrer et al., 2011; Uchimura et al., 2018). The postprandial trajectory of each metabolite ion was defined using k-means clustering to classify metabolites according to the proportional patterns of increase or decrease over time in every case after the test meal (Figure S3A). In an unsupervised clustering analysis of metabolites that showed consistent postprandial trends in at least 4 of 6 patients, we found groups of metabolites that were generally present in early fasting time points and decreased subsequently and other groups of metabolites that were increased at different times (Figure S3B; metabolite annotation: Table S3). Using The Human Metabolome Database (HMDB) (Wishart et al., 2022) and (FooDB) (The Metabolomics Innovation Centre, 2017) database, we classified the likely origin of each metabolite (Figure S3B; Table S3). Although it was ethically unacceptable to alter the patients' medication regimen for this study, most medications had been dosed by the patient in the morning before the test breakfast, and 15% of pharmaceuticals increased, whereas 8% decreased during subsequent sampling (Figure S3B). Different plant xenobiotics showed both increasing (37%) or decreasing (35%) postprandial trajectories and accounted for the largest proportion of metabolites isolated from the small intestinal output. We concluded that the dominance of plant xenobiotics and the lack of an overall proportional change in this metabolite class is consistent with the slow clearance of these non-absorbable small molecules from the small intestine.

Notably, we did not detect increases of mono- or di-saccharides following the meal: we interpreted these results as the completeness of saccharide uptake in colonized human small intestine, with consumption of any non-absorbed molecules as preferred carbon sources for bacterial growth and division. Increased bile acids were also not detected postprandially, likely reflecting binding to plant fiber (Naumann et al., 2020) and the ileal reuptake of free bile acids before distal stoma sampling (Trauner and Boyer, 2003). The small hydrodynamic volume of the $M_r < 1,000$ analytes measured by high-resolution untargeted mass-spectrometry allows diffusion and access to pores in mucus and glycocalyx layers, resulting in very limited clearance by inter-digestive intestinal peristalsis during an overnight fast. The finding of limited generalized postprandial fluctuation of individual metabolites in the distal small intestinal fluid is therefore consistent with heterogeneity in the pretest diet taken by the 6 subjects in this longitudinal study.

Differences in the metabolome in steady-state samples from stomas at different levels of the intestine

Having shown that analytes annotated as plant metabolites were present in both fasting and postprandial samples of the small intestinal output, we asked how the patterns of metabolites differ between the small intestine and the proximal or distal colon. For this, we needed to analyze stoma outputs at different levels

Figure 4. Microbial and metabolomic changes between fasting and feeding in ileostomas of treated CRC patients

(A) Box plots for metagenomic read numbers mapping to bacteria, host, archaea, or virus. See also Figure S2.

(B and C) Microbial/host DNA ratios (B) and Shannon alpha diversities (C) in ileal stomas over time. The main panel in (C) includes host DNA whereas the (C) inset panel excluded host sequences from Shannon index calculations. Each color represents an individual patient and gray bars at 2, 6, and 48 h show the first sampling time after feeding. Changes in diversity over different time points were tested using a linear-mixed-effect model with the individual as a random effect.

(D) Changes of absolute microbial mass per gram of ileal stoma contents at 2 and 4 h after breakfast assessed by bacterial flow cytometry. Each color represents a separate individual. Differences between time points were tested by paired non-parametric test corrected for multiple comparisons controlling the FDR using the two-stage linear step-up method of Benjamini, Krieger, and Yekutieli. (*adj-$p < 0.05$).

(E and F) Ordination plots show microbial (E) and metabolomic (D) distinctiveness in patients from (A) assessed by Bray-Curtis dissimilarity metrics.

(G) Microbial changes in ileal stoma samples from recovered CRC patients in (A) were assessed by metagenomic sequencing. Heatmap shows relative abundance changes over time in each patient (P1–P7).

(H) Numbers of strains within each patient that were shared (ANI > 99.999%) or non-shared (ANI < 99.999%) over different times after feeding.

(I) Genetic identity similarities of *E. coli* and *K. pneumoniae* within patients' samples or between patients' samples are shown based on PopANI values. The difference between groups was compared with an unpaired non-parametric Mann-Whitney U test. *$p < 0.05$, **$p < 0.01$, ***$p < 0.001$, and n.s., non-significant.

(J) Violin plot shows the nucleotide diversity for the most abundant species from ileal stomas in recovered color-coded CRC patients. The same color within the violin plot for a single species represents different times of sampling. The orange-shaded zone shows identical strains (ANI $\geq$ 99.999%).

31 samples from different time points (0–48 h) of 6 patients were used in these analyses except (D), which shows 12 samples from three different time points (0–4 h) of 4 independent patients after fasting overnight.

See also Figure S5.

of the intestinal tract: since each patient only has a single stoma, we therefore compared the steady-state metabolome (taken in the morning 2–4 h after breakfast) of ileal and colonic samples according to the different positions of stomas in individual patients across our CRC cohort.

Relatively few compound classes showed significant proportionate differences by untargeted metabolomics comparing 30 ileal and 49 cured CRC colonic stomas. Despite the underlying patient heterogeneity, ileostoma compared with left-sided colostoma contained relatively reduced proportions of benzenoids ($q < 0.05$), cinnamic acids/derivatives, and organoheterocyclic compounds (both $q < 0.2$) (Figures S3D and S4; Table S4). There were no significant differences in metabolite classes between the ileum and right colon in CRC patients. In contrast, benzene/substituted derivatives, benzenoids, carboxylic acids/derivatives, organic acids/derivatives, and organoheterocyclic compounds were proportionately reduced comparing the ileum and right colon of CD patients ($q < 0.01$ apart from benzene/derivatives $q < 0.05$) (Figures S3E and S4; Table S4). These proportionate compound class increases in the colon are consistent with metabolism by increased microbial biomass.

Given that approximately 36% of the persistent metabolites that we had found in the ileal metabolomic analysis were annotated as of plant origin, we also analyzed our metagenomic dataset for annotated DNA sequences from the plant kingdom (Figure S5). We reasoned that these plant DNA sequences would have been fragmented through cooking and nucleosidases during digestion. Overall, proportions of plant DNA reads, dominated by taxa from *Fabales*, *Poales*, *Gentianales*, and *Solanales* did not change significantly between fasted and fed ileostoma patients (Figure S5A). However, there were minor increases in plant DNA reads corresponding to individual plant taxa following feeding, although the taxa detected differed according to the sampled individual (Figure S5B). In one case, cannabis DNA was detected at the end of the study trajectory likely because of non-prescribed oral self-medication (Figure S5B). Therefore, like plant metabolites, plant DNA fragments are also highly persistent in the small intestine, and the proportions do not change after food, unlike the prokaryotic DNA derived from intact bacterial cells which are largely purged through fasting and bloom following a meal.

Rapid shifts of microbiota sub-strains in the distal small intestine

Microbiota analyses are commonly reported at the genus or amplicon sequence variant (ASV) level to allow scalable analyses across populations or within individuals over time. Metagenomic sequences allow annotation at the species level, although even this is an incomplete picture, as each microbial species is comprised of multiple variants (Garud et al., 2019; Schloissnig et al., 2013; Zhao et al., 2019). The metagenomic analysis of ileal microbiota showed that the biomass itself was responsive to feeding and fasting, but the overall diversity of taxa present was not. The Shannon entropy index did not show significant changes over the course of the postprandial sampling (Figure 4C inset). Although individual patients' ileal microbiotas were distinct, there were no significant differences of microbial and metabolite profiles within each individual over time as assessed by Bray-Curtis dissimilarity metrics: this indicated that all species had proportionately increased in abundance as the overall biomass increased (Figures 4E and 4F).

In an earlier study of microbiota evolution in mice, we had directly shown the emergence of different sub-strains of a dominant microbiota taxon (*B. cecimuris* I48) by sequencing single bacterial cell clones (Yilmaz et al., 2021). We also showed the emergence of different sub-strains over time and that alterations in their proportions could be indirectly inferred informatically through coordinate shifts in the allele frequencies of sets of variants on a single bacterial chromosome: in some cases, the coordinate changes were seen with overlapping but not congruent single-nucleotide polymorphisms (SNPs)—here it is likely that a parent strain, with some but not all variants, was undergoing the same shift as its progeny which had acquired additional SNPs (Yilmaz et al., 2021). The question was therefore whether there is a proportionate change of the sub-strains within each species or whether different sub-strain components bloom and contract within the niche occupied by the strain itself as intraluminal small intestinal conditions change in humans. We hypothesized that there would only be limited numbers of sub-strains that would also be reasonably stable in composition within individual taxa to ensure a sufficient burst size for each during postprandial restitution of the microbiota.

We analyzed deep metagenomic sequencing of the ileal microbiota samples with bacterial strain level assessments using the MIDAS (Nayfach et al., 2016) and inStrain (Olm et al., 2021) pipelines. Using the definition of average nucleotide identity (ANI) of 99.999% as indicating strain identity within a bacterial species, we could show by comparison of variants across individuals using "inStrain compare" that although there were more strain differences between individuals than within an individual, many taxa within each individual comprised multiple different strains and were oscillated in relative abundance over fasting and feeding cycle in one of three modes (Figures 4G–4J and S5E).

Nevertheless, there were many variants within each strain meeting the criterion of <99.999% ANI and therefore designated as sub-strains. We confirmed that such coordinate allele frequency variant shifts also occurred in fecal samples of two healthy individuals taken at 2 weekly intervals for 6 weeks (Figure 5A). Sub-strain frequencies inferred based on coordinate allele frequency shifts were highly unstable across sequential hourly samples from the ileal stomas, even in successive samples after the microbiota biomass had expanded 2 h after feeding (Figures 4B and 5B). Despite the low fasting ileal microbial biomass, in one case, we were able to carry out variant analysis in a fasting patient and follow this after feeding (Figures 5B and S6). This also showed coordinate shifts of multiple groups of allele frequencies before and after different times following feeding. Using hierarchical analysis of variant clusters, in this case, we could infer that there were more than 16 sub-strains of *E. coli* and 19 of *K. pneumoniae*, some of which reached an allele frequency of almost 100% before disappearing in subsequent samples 2–4 h later (Figures 5B and S6C; Table S5). Since the time course for these clustered allele frequency shifts is too fast for most to be accounted for by new mutations (as they would have to expand and fix coordinately in the overall population; Good et al., 2017), we interpret these changes as the rapid expansion from a sufficient burst size of the sub-strains present

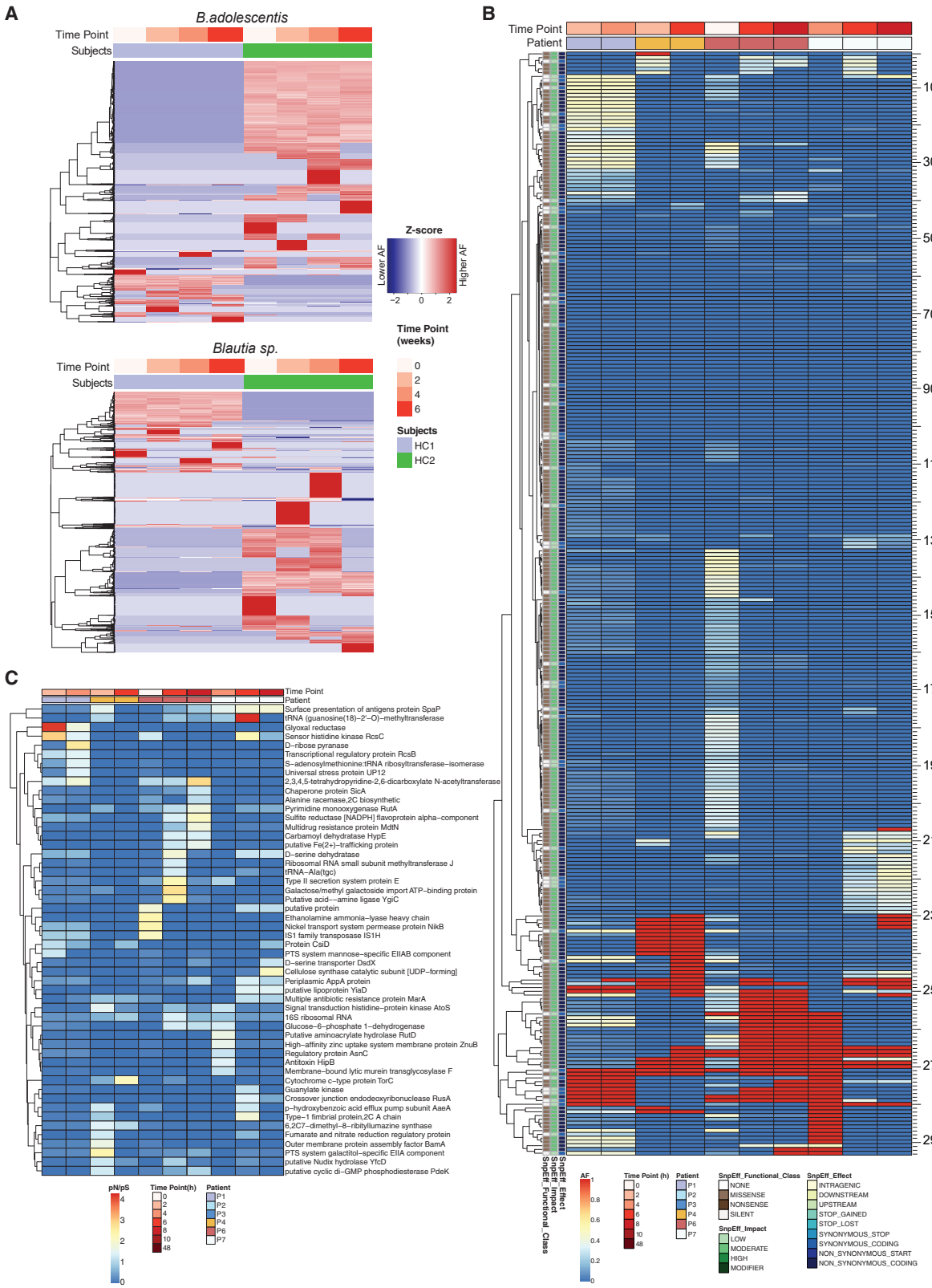

Figure 5. Sub-strains fluctuations in healthy subjects and CRC patients

(A) Metagenomic sequencing of the fecal bacterial DNA in healthy subjects was performed over 6 weeks with fortnightly sampling. Variants were called by comparison to the reference genome of each species. Variant changes over weeks are shown for *B. adolescentis* and *Blautia sp.* in two healthy individuals.

(legend continued on next page)

in the distal small intestine or transported distally—at times below detection levels at the stoma for metagenomic analysis. Contractions of sub-strains are likely mostly through distal loss into the stoma. This shows the rapid expansion (and contraction) of sub-strains that can persist at very low frequencies, at times also within a very reduced overall biomass.

Most of these sub-strain variants in both *E. coli* and *K. pneumoniae* were non-synonymous, although clusters also contained synonymous variants undergoing the same frequency shifts, likely because of linkage on the same chromosome. To infer whether there was evidence that some of these variants had previously been subject to selection events, we examined the relative rate of increase in non-synonymous versus synonymous variants through the pN/pS ratios at different loci (Olm et al., 2021; Schloissnig et al., 2013). This showed variants at some loci compatible with past positive (pN/pS > 1) selection events (Figures 5C and S6D), although the caveats are (1) that our values are calculated with respect to the reference genome rather than over evolutionary time and (2) that the functionality of the reference or variant protein products is not known.

Since bacterial structural variation (SV) regions possibly contain functional genes involved in host-microbial interactions and provide information on the sub-genome resolution of bacterial functionality, we applied "iterative coverage-based read assignment" (ICRA) and SGV-Finder (Zeevi et al., 2019) for temporal characterization of the microbial genetic differences within individuals over the fasting and feeding cycle. We specifically focused on the function of SVs in *E. coli* by searching for enriched (via increased standardized coverage of the region) or depleted genetic functions. We identified 87 deletion SVs (dSVs, Figure 6A) compared with 55 variable SVs (vSVs, Figure 6B) for *E. coli* (Table S6). Most of the dSVs and vSVs were in gene regions annotated as ABC type and other transport systems, host-targeting type IV secretion proteins, and toxin-antitoxin modules, membrane proteins, and transcriptional regulators.

Most of the genes that contain SNPs for *E. coli* have annotations for membrane transport proteins, iron uptake, lactate utilization, binding proteins, transcriptional regulation, and numerous enzymatic (e.g., oxidoreductase, synthase, transferase, dehydrogenase, ligase, aminopeptidase, reductase, permease, and endonuclease) activities (Figure 5B; Table S5). These functions are also observed in SV analysis (Figure 6B), with some SNPs identified located in the same gene regions of identified dSVs or vSVs (Figure 6; Table S6: Del3, Del12, Del25, Del66, Del83, EfeO, DgcM, ObgE/CgtA, and Var32). The significance of changes in these functions is only by inference but would be consistent with possible adaptation (or exaptation) and fitness in the dynamic small intestinal environment. In addition, phage- and transposon-related genes and phage integrase genes were enriched or depleted over time in SVs, suggesting that these generated variants may contribute to phenotypic heterogeneity with the potential for increasing motility and viability via interacting with their environment without a change in overall gene content. In one patient (#6, Figure 6), where sequencing depth allowed analysis even in the relatively limited fasting microbial biomass, 27/54 dSVs became undetectable and 10 appeared in the postprandial period.

We concluded that there are therefore two types of microbiota instability in the distal small intestine of ileostoma patients. (1) The overall microbial ileal biomass contracts in the inter-digestive period and blooms again after the patient eats, and (2) variant sub-strains within individual taxa that (although the proportions of the taxa show coordinate changes during biomass expansion) are highly unstable over time, even during the digestive period in the fed patient.

DISCUSSION

We have studied patients who had recovered from their original disease with surgically fashioned stomas that allow real-time access to the distal small intestine and different levels of the large intestine without purgatives or other clinical manipulations. Our data show that there are potentially two types of instability in the host-microbial interaction. First, the biomass in the distal small intestine is substantially shed in ileostomas following a fasting period and rapidly blooms in the fed state. Second, the proportions of different taxa in the large intestine are stable, and there are only minor changes in taxa proportions in the distal small intestine. Beneath this stability, there are coordinate alterations of different clusters of allele frequencies within a strain, occurring with a very rapid dynamic during the digestive period in the small intestine. This is consistent with multiple sub-strains changing rapidly over time. The very rapid timing of sub-strain appearance and disappearance in the small intestine is compatible with blooms and contractions of the sub-strains concerned, in some cases with very large changes in allele frequency and contraction to undetectable levels. Although the different taxa of the colonic human microbiota are normally found to be quite stable in adulthood, our data in the disconnected distal small intestine shows that this apparent stability can conceal components of extremely rapid dynamics, even occurring within a period of several hours.

In contrast to the rapid dynamics of the microbiota, many small metabolites only show minor proportional differences in the small intestine after feeding and between the different sites along the intestine. These more limited dynamics are consistent with the slower passage of small metabolites (M_r < 1,000) along the intestinal tract with its substantial unstirred compartment.

How representative are these data for the healthy human ileum in the absence of surgical manipulation or the illness that preceded it? We found no significant differences over time in alpha or beta diversities comparing samples of the ileal contents taken directly during surgery before the ileostoma was fashioned and those taken later from the ileostoma itself. Since we and others

(B) Variants with unsupervised clustering from ileal stomas for *E. coli* after feeding as in Figure 5. Time points after breakfast and patient identities are shown above the heatmap.

(C) Genes with sufficient sequencing depth with pN/pS ratios inferring a history of positive (>1) selection events in patients from (B). SnpEff annotation of non-synonymous and synonymous mutations.

(A) contains 8 samples from 2 healthy individuals. (B) and (C) contain 10 samples from different time points (0–48 h) of 4 patients.

See also Figure S6.

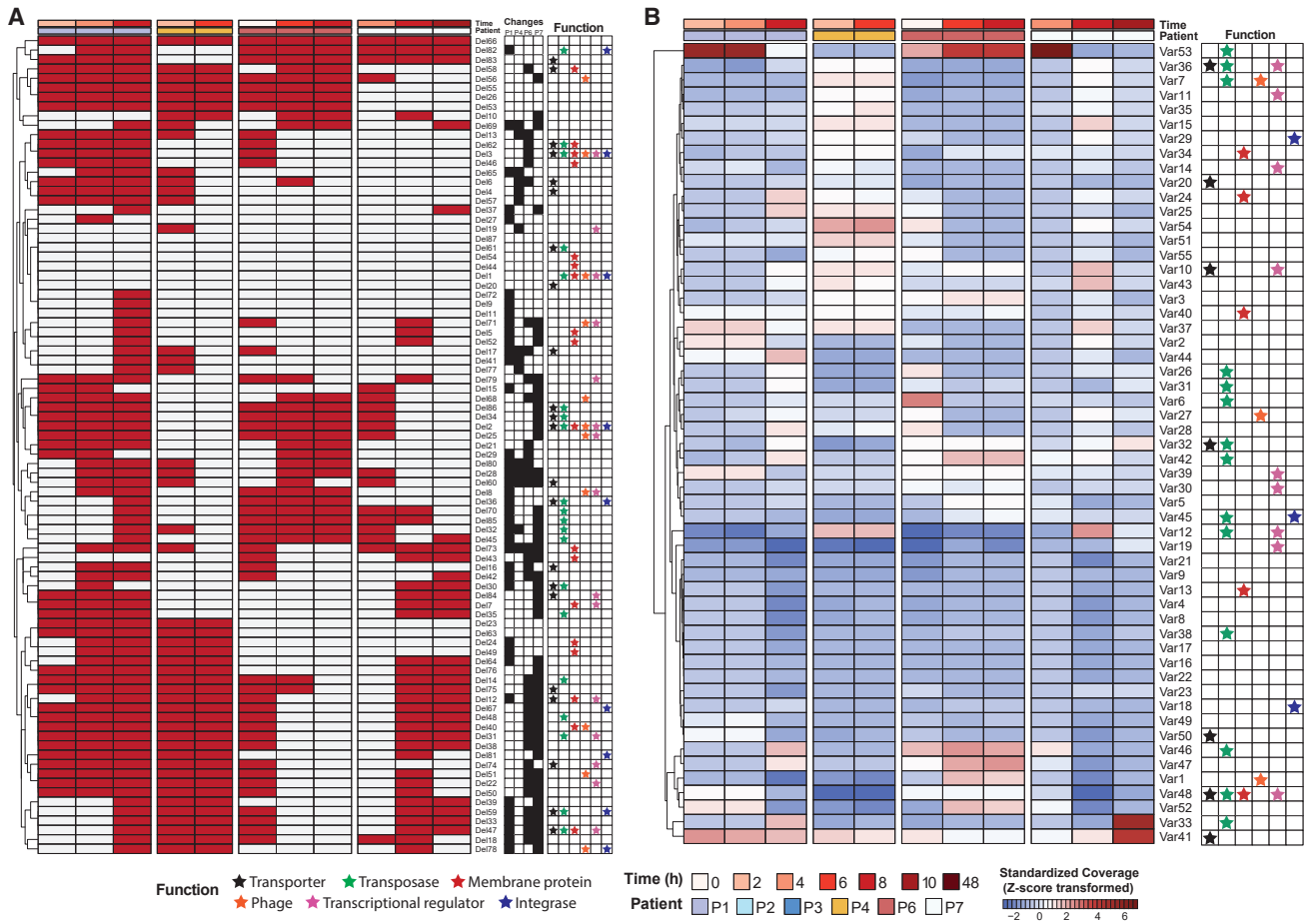

Figure 6. Postprandial variability in structural variations in *E. coli*

(A) Heatmap shows deletion SVs from ileal stomas for *E. coli* after feeding.

(B) Heatmap shows variable SVs in *E. coli* after feeding.

(A) and (B) contains 11 samples from different time points (0–48 h) of 4 patients. The presence (red) and absence (gray) of deletion SVs are shown in (A). Deletions in genomic locations are annotated based on their functional categories and are shown with stars on the right side of the heatmap.

See also Table S6.

have shown that there are persistent alterations in the microbiota of CD patients following surgery (Fang et al., 2021; Yilmaz et al., 2019), so we excluded patients with IBD for longitudinal ileostoma studies and prioritized cured CRC patients in our studies. The cured CRC colonic microbiota does contain altered bacterial populations (Dai et al., 2018) but unlike CD, the terminal ileum is normally not involved in colon cancer. Nevertheless, a persistent effect on the small intestinal microbiota during or after stoma formation cannot be excluded.

Our data on biomass and inferred sub-strain fluctuations in the fed-fasting cycle come entirely from luminal contents of the disconnected ileostoma in patients treated for distal colon cancer. Disconnection of the fecal stream has been shown not to increase the ileal fluid flux (Ladas et al., 1986), and the taxa we find in the microbiota are broadly consistent with earlier qPCR results in mucosal biopsies obtained in 6 emergency surgical patients (Ahmed et al., 2007) and by colonoscopic aspiration following ileostoma closure in intestinal transplant patients (Hartman et al., 2009). This suggests that the inter-digestive microbial load from the small intestine is likely also true of normal subjects with an intact intestine. Studies of the ileocecal valve, which anatomically separates the small and large intestines, are also limited by accessibility, but both human and large animal studies indicate that a functional high-pressure zone avoids free reflux of large intestinal contents (Dinning and Hixson, 1995), with neuromuscular control allowing drainage of small intestinal contents both in digestive and inter-digestive phases (Malbert, 2005).

Since the ileum is proximal to the main biomass of the colonic microbiota, ileal microbiota alterations may also contribute to shaping the composition of the large intestinal microbiota. We were also able to show allele frequency variations compatible with sub-strain fluctuations in fecal samples of control patients (with an intact intestinal tract).

SVs within human intestinal microbiome species have been described within individual subjects across time. They are also more common between unrelated cohabitants than in different individuals living apart. Some of these SVs are positively or negatively associated with the health metrics (Zeevi et al., 2019). In elderly patients, it can be detrimental to lose microbiota species diversity, and in some cases, replacements by

exotic taxa can provide health benefits (Wilmanski et al., 2021). The human gut microbiota may evolve with short-term evolutionary dynamics (albeit with human-relevant timescales) and longer-term evolution across hosts. If one considers the human gut as a unit, many microbial species are not a genetically cohesive population: rather, there are genetically distinct collections of lineages within the same individual (Garud et al., 2019). Our data from human terminal ileal stomas support this for a particular segment of the intestinal tract that is subject to wide variations in microbial biomass over the digestive and inter-digestive cycles and indicate that there can also be rapid changes in the lineage composition of individual taxa. Given that SVs within microbial species are more common in transport systems than genes for core metabolic pathways and can be associated with a growth advantage (Zeevi et al., 2019), the timescale of hours over which allele frequencies of the inferred sub-strains change indicates that these rapid changes are driven by changing intraluminal ecological conditions rather than *de novo* mutations.

We therefore propose that large numbers of dynamic sub-strain ecotypes within individual microbial taxa of the distal small intestine are a normal feature of healthy host-microbial mutualism, allowing homeostasis to be maintained in a wide range of intraluminal conditions, where individual taxa are stabilized by alterations in their sub-species proportions carrying relevant functional variants. This may avoid alpha diversity loss and dysbiosis unless bottlenecks occur associated with disease, diet, or environmental pressures. Our ecosystems biology approach using molecular datasets (Raes and Bork, 2008) from stoma patient samples supports the flexibility of the sub-strain structure of the small intestinal microbiota and its potential to adapt its biomass according to phases of dietary intake.

STAR★METHODS

Detailed methods are provided in the online version of this paper and include the following:

- KEY RESOURCES TABLE
- RESOURCE AVAILABILITY
  - Lead Contact
  - Materials availability
  - Data and code availability
- EXPERIMENTAL MODEL AND SUBJECT DETAILS
  - Study design
  - Ethics statement
- METHOD DETAILS
  - Sample collection
  - DNA extraction from human intestinal biopsies and luminal contents
  - 16S amplicon sequencing using IonTorrent PGM platform
  - Determination of the biomass
  - Metabolomics
  - Library preparation and sequencing for metagenomics
  - *The inStrain* pipeline
  - Variant annotation
  - Structural variation identification and annotation
- QUANTIFICATION AND STATISTICAL ANALYSIS

SUPPLEMENTAL INFORMATION

Supplemental information can be found online at https://doi.org/10.1016/j.chom.2022.10.002.

ACKNOWLEDGMENTS

We thank the staff of Inselspital for technical and financial support. We are grateful to Dr. Peter Studer and Dr. Pascal Juillerat for sample collections and Dr. Ruben Mars for metabolic sample processing. We are thankful to the University of Bern NGS Platform for metagenomic sequencing. This work was supported by the Swiss National Science Foundation (SNF Sinergia CRSII3_154414 and SNF Sinergia CRSII5_177164 to A.J.M.; SNF Ambizione Grant PZ00P3_185880 to B.Y. and SNF Grant 320030_197815 to B.M.) A.J.M. was supported by European Research Council (HHMM-Neonates Project Number: 742195). A.J.M. and B.Y. were also supported by Bern Center for Precision Medicine (BCPM), University of Bern.

AUTHOR CONTRIBUTIONS

Conceptualization, A.J.M. and B.Y.; investigation, B.Y., A.J.M., D.M., T.F., N.K., D.S., D.C., G.B., B.M., and U.S.; data analysis, B.Y., A.J.M., T.F., and D.W.; resources, A.J.M.; writing – original draft, A.J.M. and B.Y.; writing – review & editing, A.J.M., and B.Y.; funding acquisition, A.J.M., B.Y., and U.S.

DECLARATION OF INTERESTS

The authors declare no competing interests.

INCLUSION AND DIVERSITY

We support inclusive, diverse, and equitable conduct of research.

Received: April 20, 2022
Revised: July 18, 2022
Accepted: October 4, 2022
Published: October 31, 2022

REFERENCES

Ahmed, S., Macfarlane, G.T., Fite, A., McBain, A.J., Gilbert, P., and Macfarlane, S. (2007). Mucosa-associated bacterial diversity in relation to human terminal ileum and colonic biopsy samples. Appl. Environ. Microbiol. *73*, 7435–7442.

Andrews, S. (2015). A quality control tool for high throughput sequence data. http://www.bioinformatics.babraham.ac.uk/projects/fastqc.

Aziz, R.K., Bartels, D., Best, A.A., DeJongh, M., Disz, T., Edwards, R.A., Formsma, K., Gerdes, S., Glass, E.M., Kubal, M., et al. (2008). The RAST Server: rapid annotations using subsystems technology. BMC Genomics *9*, 75.

Bäckhed, F., Roswall, J., Peng, Y., Feng, Q., Jia, H., Kovatcheva-Datchary, P., Li, Y., Xia, Y., Xie, H., Zhong, H., et al. (2015). Dynamics and stabilization of the human gut microbiome during the first year of life. Cell Host Microbe *17*, 690–703.

Bentley, D.W., Nichols, R.L., Condon, R.E., and Gorbach, S.L. (1972). The microflora of the human ileum and intrabdominal colon: results of direct needle aspiration at surgery and evaluation of the technique. J. Lab. Clin. Med. *79*, 421–429.

Booijink, C.C.G.M., El-Aidy, S., Rajilić-Stojanović, M., Heilig, H.G.H.J., Troost, F.J., Smidt, H., Kleerebezem, M., De Vos, W.M.D., and Zoetendal, E.G. (2010). High temporal and inter-individual variation detected in the human ileal microbiota. Environ. Microbiol. *12*, 3213–3227.

Byndloss, M.X., Olsan, E.E., Rivera-Chávez, F., Tiffany, C.R., Cevallos, S.A., Lokken, K.L., Torres, T.P., Byndloss, A.J., Faber, F., Gao, Y., et al. (2017). Microbiota-activated PPAR-gamma signaling inhibits dysbiotic Enterobacteriaceae expansion. Science *357*, 570–575.

Callahan, B.J., Sankaran, K., Fukuyama, J.A., McMurdie, P.J., and Holmes, S.P. (2016). Bioconductor workflow for microbiome Data Analysis: from raw reads to community analyses. F1000Res *5*, 1492.

Caporaso, J.G., Kuczynski, J., Stombaugh, J., Bittinger, K., Bushman, F.D., Costello, E.K., Fierer, N., Peña, A.G., Goodrich, J.K., Gordon, J.I., et al. (2010). QIIME allows analysis of high-throughput community sequencing data. Nat. Methods *7*, 335–336.

Cingolani, P., Platts, A., Wang, L.L., Coon, M., Nguyen, T., Wang, L., Land, S.J., Lu, X., and Ruden, D.M. (2012). A program for annotating and predicting the effects of single nucleotide polymorphisms, SnpEff: SNPs in the genome of Drosophila melanogaster strain w1118; iso-2; iso-3. Fly (Austin) *6*, 80–92.

Cooper, J.C., Laughland, A., Gunning, E.J., Burkinshaw, L., and Williams, N.S. (1986). Body composition in ileostomy patients with and without ileal resection. Gut *27*, 680–685.

Dai, Z., Coker, O.O., Nakatsu, G., Wu, W.K.K., Zhao, L., Chen, Z., Chan, F.K.L., Kristiansen, K., Sung, J.J.Y., Wong, S.H., et al. (2018). Multi-cohort analysis of colorectal cancer metagenome identified altered bacteria across populations and universal bacterial markers. Microbiome *6*, 70.

Danecek, P., Auton, A., Abecasis, G., Albers, C.A., Banks, E., DePristo, M.A., Handsaker, R.E., Lunter, G., Marth, G.T., Sherry, S.T., McVean, G., Durbin, R., and Genomes Project Analysis, G. (2011). The variant call format and VCFtools. Bioinformatics *27*, 2156–2158.

Dinning, J.P., and Hixson, L.J. (1995). Value of flexible Sigmoldoscopy – reply. Arch. Intern. Med. *155*, 427.

Donaldson, G.P., Lee, S.M., and Mazmanian, S.K. (2016). Gut biogeography of the bacterial microbiota. Nat. Rev. Microbiol. *14*, 20–32.

Drasar, B.S., and Shiner, M. (1969). Studies on the intestinal flora. II. Bacterial flora of the small intestine in patients with gastrointestinal disorders. Gut *10*, 812–819.

Duffy, M., O'Mahony, L., Coffey, J.C., Collins, J.K., Shanahan, F., Redmond, H.P., and Kirwan, W.O. (2002). Sulfate-reducing bacteria colonize pouches formed for ulcerative colitis but not for familial adenomatous polyposis. Dis. Colon Rectum *45*, 384–388.

Englyst, H.N., and Cummings, J.H. (1987). Digestion of polysaccharides of potato in the small intestine of man. Am. J. Clin. Nutr. *45*, 423–431.

Faith, J.J., Guruge, J.L., Charbonneau, M., Subramanian, S., Seedorf, H., Goodman, A.L., Clemente, J.C., Knight, R., Heath, A.C., Leibel, R.L., et al. (2013). The long-term stability of the human gut microbiota. Science *341*, 1237439.

Fang, X., Vázquez-Baeza, Y., Elijah, E., Vargas, F., Ackermann, G., Humphrey, G., Lau, R., Weldon, K.C., Sanders, J.G., Panitchpakdi, M., et al. (2021). Gastrointestinal surgery for inflammatory bowel disease persistently lowers microbiome and metabolome diversity. Inflamm. Bowel Dis. *27*, 603–616.

Finegold, S.M., Sutter, V.L., Boyle, J.D., and Shimada, K. (1970). The normal flora of ileostomy and transverse colostomy effluents. J. Infect. Dis. *122*, 376–381.

Finegold, S.M., Sutter, V.L., and Mathisen, G.E. (1983). Normal indigenous intestinal flora. In Human intestinal microflora in health and disease, D. Hentges, ed. (Academic Press), pp. 3–31.

Florin, T.H., Neale, G., and Cummings, J.H. (1990). The effect of dietary nitrate on nitrate and nitrite excretion in man. Br. J. Nutr. *64*, 387–397.

Fuhrer, T., Heer, D., Begemann, B., and Zamboni, N. (2011). High-throughput, accurate mass metabolome profiling of cellular extracts by flow injection-time-of-flight mass spectrometry. Anal. Chem. *83*, 7074–7080.

Fuhrer, T., Zampieri, M., Sévin, D.C., Sauer, U., and Zamboni, N. (2017). Genomewide landscape of gene-metabolome associations in *Escherichia coli*. Mol. Syst. Biol. *13*, 907.

Garud, N.R., Good, B.H., Hallatschek, O., and Pollard, K.S. (2019). Evolutionary dynamics of bacteria in the gut microbiome within and across hosts. PLoS Biol. *17*, e3000102.

Good, B.H., McDonald, M.J., Barrick, J.E., Lenski, R.E., and Desai, M.M. (2017). The dynamics of molecular evolution over 60,000 generations. Nature *551*, 45–50.

Gorbach, S.L., Nahas, L., Weinstein, L., Levitan, R., and Patterson, J.F. (1967). Studies of intestinal microflora. IV. The microflora of ileostomy effluent: a unique microbial ecology. Gastroenterology *53*, 874–880.

Hartman, A.L., Lough, D.M., Barupal, D.K., Fiehn, O., Fishbein, T., Zasloff, M., and Eisen, J.A. (2009). Human gut microbiome adopts an alternative state following small bowel transplantation. Proc. Natl. Acad. Sci. USA *106*, 17187–17192.

Hill, M.J. (2020). Factors controlling the microflora of the healthy upper gastrointestinal tract. In Human microbial ecology (CRC Press), pp. 57–85.

Hill, M.J., and Marsh, P.D. (1989). Human microbial ecology (CRC Press).

Holmes, E., Li, J.V., Athanasiou, T., Ashrafian, H., and Nicholson, J.K. (2011). Understanding the role of gut microbiome-host metabolic signal disruption in health and disease. Trends Microbiol. *19*, 349–359.

Hooper, L.V., Wong, M.H., Thelin, A., Hansson, L., Falk, P.G., and Gordon, J.I. (2001). Molecular analysis of commensal host-microbial relationships in the intestine. Science *291*, 881–884.

Köster, J., and Rahmann, S. (2012). Snakemake–a scalable bioinformatics workflow engine. Bioinformatics *28*, 2520–2522.

Ladas, S.D., Isaacs, P.E., Murphy, G.M., and Sladen, G.E. (1986). Fasting and postprandial ileal function in adapted ileostomates and normal subjects. Gut *27*, 906–912.

Livesey, G., Wilkinson, J.A., Roe, M., Faulks, R., Clark, S., Brown, J.C., Kennedy, H., and Elia, M. (1995). Influence of the physical form of barley grain on the digestion of its starch in the human small intestine and implications for health. Am. J. Clin. Nutr. *61*, 75–81.

Lou, Y.C., Olm, M.R., Diamond, S., Crits-Christoph, A., Firek, B.A., Baker, R., Morowitz, M.J., and Banfield, J.F. (2021). Infant gut strain persistence is associated with maternal origin, phylogeny, and traits including surface adhesion and iron acquisition. Cell Rep. Med. *2*, 100393.

Lu, J., Breitwieser, F.P., Thielen, P., and Salzberg, S.L. (2017). Bracken: estimating species abundance in metagenomics data. PeerJ *3*, e104.

Macfarlane, G.T., and Englyst, H.N. (1986). Starch utilization by the human large intestinal microflora. J. Appl. Bacteriol. *60*, 195–201.

Madsen, J.L., Søndergaard, S.B., and Møller, S. (2006). Meal-induced changes in splanchnic blood flow and oxygen uptake in middle-aged healthy humans. Scand. J. Gastroenterol. *41*, 87–92.

Malbert, C.H. (2005). The ileocolonic sphincter. Neurogastroenterol. Motil. *17* (*Suppl 1*), 41–49.

Mallick, H., Rahnavard, A., McIver, L.J., Ma, S., Zhang, Y., Nguyen, L.H., Tickle, T.L., Weingart, G., Ren, B., Schwager, E.H., et al. (2021). Multivariable association discovery in population-scale meta-omics studies. PLoS Comput. Biol. *17*, e1009442.

Martin, S.T., and Vogel, J.D. (2012). Intestinal stomas: indications, management, and complications. Adv. Surg. *46*, 19–49.

McKenna, A., Hanna, M., Banks, E., Sivachenko, A., Cibulskis, K., Kernytsky, A., Garimella, K., Altshuler, D., Gabriel, S., Daly, M., and DePristo, M.A. (2010). The Genome Analysis Toolkit: a MapReduce framework for analyzing next-generation DNA sequencing data. Genome Res. *20*, 1297–1303.

McMurdie, P.J., and Holmes, S. (2013). phyloseq: an R package for Reproducible Interactive Analysis and Graphics of microbiome Census Data. PLoS One *8*, e61217.

McMurdie, P.J., and Holmes, S. (2014). Waste not, want not: why rarefying microbiome data is inadmissible. PLoS Comput. Biol. *10*, e1003531.

Mende, D.R., Letunic, I., Huerta-Cepas, J., Li, S.S., Forslund, K., Sunagawa, S., and Bork, P. (2017). proGenomes: a resource for consistent functional and taxonomic annotations of prokaryotic genomes. Nucleic Acids Res. *45*, D529–D534.

Miller, M.A., Parkman, H.P., Urbain, J.L., Brown, K.L., Donahue, D.J., Knight, L.C., Maurer, A.H., and Fisher, R.S. (1997). Comparison of scintigraphy and lactulose breath hydrogen test for assessment of orocecal transit: lactulose accelerates small bowel transit. Dig. Dis. Sci. *42*, 10–18.

Morgan, X.C., Tickle, T.L., Sokol, H., Gevers, D., Devaney, K.L., Ward, D.V., Reyes, J.A., Shah, S.A., LeLeiko, N., Snapper, S.B., et al. (2012).

Dysfunction of the intestinal microbiome in inflammatory bowel disease and treatment. Genome Biol. *13*, R79.

Naumann, S., Haller, D., Eisner, P., and Schweiggert-Weisz, U. (2020). Mechanisms of interactions between bile acids and plant compounds-A review. Int. J. Mol. Sci. *21*.

Nayfach, S., Rodriguez-Mueller, B., Garud, N., and Pollard, K.S. (2016). An integrated metagenomics pipeline for strain profiling reveals novel patterns of bacterial transmission and biogeography. Genome Res. *26*, 1612–1625.

Olm, M.R., Crits-Christoph, A., Bouma-Gregson, K., Firek, B.A., Morowitz, M.J., and Banfield, J.F. (2021). inStrain profiles population microdiversity from metagenomic data and sensitively detects shared microbial strains. Nat. Biotechnol. *39*, 727–736.

Padmanabhan, P., Grosse, J., Asad, A.B., Radda, G.K., and Golay, X. (2013). Gastrointestinal transit measurements in mice with 99mTc-DTPA-labeled activated charcoal using NanoSPECT-CT. EJNMMI Res. *3*, 60.

Pomare, E.W., Branch, W.J., and Cummings, J.H. (1985). Carbohydrate fermentation in the human colon and its relation to acetate concentrations in venous blood. J. Clin. Invest. *75*, 1448–1454.

Proano, M., Camilleri, M., Phillips, S.F., Brown, M.L., and Thomforde, G.M. (1990). Transit of solids through the human colon: regional quantification in the unprepared bowel. Am. J. Physiol. *258*, G856–G862.

Pruesse, E., Quast, C., Knittel, K., Fuchs, B.M., Ludwig, W., Peplies, J., and Glöckner, F.O. (2007). SILVA: a comprehensive online resource for quality checked and aligned ribosomal RNA sequence data compatible with ARB. Nucleic Acids Res. *35*, 7188–7196.

Raes, J., and Bork, P. (2008). Molecular eco-systems biology: towards an understanding of community function. Nat. Rev. Microbiol. *6*, 693–699.

Rotmistrovsky, K., and Agarwala, R. (2011). BMTagger: best match tagger for removing human reads from metagenomics datasets. ftp://ftp.ncbi.nlm.nih.gov/pub/agarwala/bmtagger/.

Schloissnig, S., Arumugam, M., Sunagawa, S., Mitreva, M., Tap, J., Zhu, A., Waller, A., Mende, D.R., Kultima, J.R., Martin, J., et al. (2013). Genomic variation landscape of the human gut microbiome. Nature *493*, 45–50.

Sévin, D.C., Fuhrer, T., Zamboni, N., and Sauer, U. (2017). Nontargeted in vitro metabolomics for high-throughput identification of novel enzymes in Escherichia coli. Nat. Methods *14*, 187–194.

Silvester, K.R., Englyst, H.N., and Cummings, J.H. (1995). Ileal recovery of starch from whole diets containing resistant starch measured in vitro and fermentation of ileal effluent. Am. J. Clin. Nutr. *62*, 403–411.

Stappenbeck, T.S., Hooper, L.V., and Gordon, J.I. (2002). Developmental regulation of intestinal angiogenesis by indigenous microbes via Paneth cells. Proc. Natl. Acad. Sci. USA *99*, 15451–15455.

Stolaki, M., Minekus, M., Venema, K., Lahti, L., Smid, E.J., Kleerebezem, M., and Zoetendal, E.G. (2019). Microbial communities in a dynamic in vitro model for the human ileum resemble the human ileal microbiota. FEMS Microbiol. Ecol. *95*, fiz096.

Sundberg, B., Wood, P., Lia, A., Andersson, H., Sandberg, A.S., Hallmans, G., and Aman, P. (1996). Mixed-linked beta-glucan from breads of different cereals is partly degraded in the human ileostomy model. Am. J. Clin. Nutr. *64*, 878–885.

Sundquist, A., Bigdeli, S., Jalili, R., Druzin, M.L., Waller, S., Pullen, K.M., El-Sayed, Y.Y., Taslimi, M.M., Batzoglou, S., and Ronaghi, M. (2007). Bacterial flora-typing with targeted, chip-based Pyrosequencing. BMC Microbiol. *7*, 108.

The Metabolomics Innovation Centre (2017). FooDB version 1.0, Computer software (The Metabolomics Innovation Centre).

Trauner, M., and Boyer, J.L. (2003). Bile salt transporters: molecular characterization, function, and regulation. Physiol. Rev. *83*, 633–671.

Uchimura, Y., Fuhrer, T., Li, H., Lawson, M.A., Zimmermann, M., Yilmaz, B., Zindel, J., Ronchi, F., Sorribas, M., Hapfelmeier, S., et al. (2018). Antibodies set boundaries limiting microbial metabolite penetration and the resultant mammalian Host Response. Immunity *49*, 545–559.e5.

Uritskiy, G.V., DiRuggiero, J., and Taylor, J. (2018). MetaWRAP-a flexible pipeline for genome-resolved metagenomic data analysis. Microbiome *6*, 158.

van Trijp, M.P.H., Rösch, C., An, R., Keshtkar, S., Logtenberg, M.J., Hermes, G.D.A., Zoetendal, E.G., Schols, H.A., and Hooiveld, G.J.E.J. (2020). Fermentation kinetics of selected dietary fibers by human small intestinal microbiota depend on the type of fiber and subject. Mol. Nutr. Food Res. *64*, e2000455.

Walker, B.J., Abeel, T., Shea, T., Priest, M., Abouelliel, A., Sakthikumar, S., Cuomo, C.A., Zeng, Q., Wortman, J., Young, S.K., and Earl, A.M. (2014). Pilon: an integrated tool for comprehensive microbial variant detection and genome assembly improvement. PLoS One *9*, e112963.

Wilm, A., Aw, P.P., Bertrand, D., Yeo, G.H., Ong, S.H., Wong, C.H., Khor, C.C., Petric, R., Hibberd, M.L., and Nagarajan, N. (2012). LoFreq: a sequence-quality aware, ultra-sensitive variant caller for uncovering cell-population heterogeneity from high-throughput sequencing datasets. Nucleic Acids Res *40*, 11189–11201.

Wilmanski, T., Diener, C., Rappaport, N., Patwardhan, S., Wiedrick, J., Lapidus, J., Earls, J.C., Zimmer, A., Glusman, G., Robinson, M., et al. (2021). Gut microbiome pattern reflects healthy aging and predicts survival in humans. Nat. Metab. *3*, 274–286.

Wishart, D.S., Guo, A., Oler, E., Wang, F., Anjum, A., Peters, H., Dizon, R., Sayeeda, Z., Tian, S., Lee, B.L., et al. (2022). HMDB 5.0: the human metabolome database for 2022. Nucleic Acids Res. *50*, D622–D631.

Wishart, D.S., Jewison, T., Guo, A.C., Wilson, M., Knox, C., Liu, Y., Djoumbou, Y., Mandal, R., Aziat, F., Dong, E., et al. (2013). HMDB 3.0–the human metabolome database in 2013. Nucleic Acids Res. *41*, D801–D807.

Wood, D.E., Lu, J., and Langmead, B. (2019). Improved metagenomic analysis with Kraken 2. Genome Biol. *20*, 257.

Wood, D.E., and Salzberg, S.L. (2014). Kraken: ultrafast metagenomic sequence classification using exact alignments. Genome Biol. *15*, R46.

Yilmaz, B., Juillerat, P., Øyås, O., Ramon, C., Bravo, F.D., Franc, Y., Fournier, N., Michetti, P., Mueller, C., Geuking, M., et al. (2019). Microbial network disturbances in relapsing refractory Crohn's disease. Nat. Med. *25*, 323–336.

Yilmaz, B., Mooser, C., Keller, I., Li, H., Zimmermann, J., Bosshard, L., Fuhrer, T., Gomez de Agüero, M., Trigo, N.F., Tschanz-Lischer, H., et al. (2021). Long-term evolution and short-term adaptation of microbiota strains and sub-strains in mice. Cell Host Microbe *29*, 650–663.e9.

Zeevi, D., Korem, T., Godneva, A., Bar, N., Kurilshikov, A., Lotan-Pompan, M., Weinberger, A., Fu, J., Wijmenga, C., Zhernakova, A., et al. (2019). Structural variation in the gut microbiome associates with host health. Nature *568*, 43–48.

Zhao, S., Lieberman, T.D., Poyet, M., Kauffman, K.M., Gibbons, S.M., Groussin, M., Xavier, R.J., and Alm, E.J. (2019). Adaptive evolution within gut microbiomes of healthy people. Cell Host Microbe *25*, 656–667.e8.

Zoetendal, E.G., Raes, J., van den Bogert, B., Arumugam, M., Booijink, C.C., Troost, F.J., Bork, P., Wels, M., de Vos, W.M., and Kleerebezem, M. (2012). The human small intestinal microbiota is driven by rapid uptake and conversion of simple carbohydrates. ISME J. *6*, 1415–1426.

STAR★METHODS

KEY RESOURCES TABLE

REAGENT or RESOURCE	SOURCE	IDENTIFIER
Chemicals, Peptides, and Recombinant Proteins		
Syto9	ThermoFisher	Cat#:S34854
Critical Commercial Assays		
PowerFecal Pro Kit	Qiagen	Cat#:51804
QIAquick Gel Extraction Kit	Qiagen	Cat#:28704
Ion PGM HiQ View Sequencing 400 kit	ThermoFisher	Cat#:A30044
RNase-free DNase Kit	Qiagen	Cat#:79254
RNeasy MinElute Cleanup Kit	Qiagen	Cat#:74204
Fluoresbrite BB Carboxylate microsphere beads	Polysciences	Cat#:19392
Qubit RNA BR Assay Kit	Thermo Fisher Scientific	Cat#:Q10211
Fragment Analyzer DNA Kit	Agilent	Cat#:5191-6570
TruSeq Stranded mRNA Library Prep	Illumina	Cat#:20020595
NovaSeq 6000 S1 Reagent Kit v1.5 (300 cycles)	Illumina	Cat#:20028317
Deposited Data		
Metabolomics Raw Data	This paper	https://figshare.com/s/5f84cf321e731a49ae06
Metagenomic Raw Sequencing Data	This paper	PRJNA825696
16S rRNA Amplicon Sequencing Data	This paper	https://figshare.com/s/077130437ca8ac314386
Oligonucleotides		
5'-CCTCTCTATGGGCAGTCG GTGATACGAGCTGACGACA RCCATG-3'	Yilmaz et al., 2019	N/A
5'-CCATCTCATCCCTGCG TGTCTCCGACTCAG-BARCODE-ATTAGATACCC YGGTAGTCC-3	Yilmaz et al., 2019	N/A
Software and Algorithms		
QIIME v1.9.1	Caporaso et al., 2010	http://qiime.org
R (v3.6.2)	Packages for analytical parts: tidyverse, ape, vegan, nlme, stats, DEseq2, edgeR, ggtree	https://www.r-project.org/
MaAsLin2	Morgan et al., 2012	https://huttenhower.sph.harvard.edu/maaslin/
Phyloseq	Callahan et al., 2016; McMurdie and Holmes, 2013	https://joey711.github.io/phyloseq/
usearch61_ref v.6.1.544	N/A	https://github.com/attayeb/auto-q
Pilon v. 1.22	Walker et al., 2014	https://github.com/broadinstitute/pilon
LoFreq v. 2.1.3.1	Wilm et al., 2012	https://bioweb.pasteur.fr/packages/pack@lofreq@2.1.3.1
vcftools v. 0.1.15	Danecek et al., 2011	https://pubmed.ncbi.nlm.nih.gov/21653522/
SnpEff v. 4.3T	Cingolani et al., 2012	https://pcingola.github.io/SnpEff/adds/SnpEff_paper.pdf
snakemake 5.3.0	Köster and Rahmann, 2012	https://snakemake.readthedocs.io/en/v5.3.0/search.html

(*Continued on next page*)

Continued

REAGENT or RESOURCE	SOURCE	IDENTIFIER
Graphpad Prism v9.0a	www.graphpad.com	https://ggplot2.tidyverse.org/index.html
Bowtie2	Langmead and Salzberg, 2012	http://bowtie-bio.sourceforge.net/bowtie2/index.shtml
GATK v.3.7	McKenna et al., 2010	https://gatk.broadinstitute.org/hc/en-us
FlowJo v10.1	Tree Star	https://www.flowjo.com
RAST	Aziz et al., 2008	https://rast.nmpdr.org
FASTQC	Andrews, 2015	https://www.bioinformatics.babraham.ac.uk/projects/fastqc/
BMTagger	Rotmistrovsky and Agarwala, 2011	https://www.westgrid.ca/support/software/bmtagger
inStrain	Olm et al., 2021	https://instrain.readthedocs.io/en/latest
Kraken2	Wood et al., 2019	https://ccb.jhu.edu/software/kraken2/
Bracken	Lu et al., 2017	https://ccb.jhu.edu/software/bracken/
SILVA 16S rRNA sequence database	Pruesse et al., 2007	https://www.arb-silva.de/
Hierarchical All-against-All (HAllA)	Huttenhower Lab	https://huttenhower.sph.harvard.edu/halla/
SGVFinder	Zeevi et al., 2019	https://github.com/segalab/SGVFinder
Progenomes	Mende et al., 2017	http://progenomes1.embl.de

RESOURCE AVAILABILITY

Lead Contact

Further information and requests for resources and reagents should be directed to and will be fulfilled by the lead contact, Andrew Macpherson (andrew.macpherson@dbmr.unibe.ch).

Materials availability

This study did not generate new unique reagents.

Data and code availability

- The data presented in this manuscript are tabulated in the main paper and the supplementary materials. All sequencing data generated in the preparation of this manuscript has been deposited in https://www.ncbi.nlm.nih.gov/bioproject/ with BioProject Accession PRJNA825696 (Accession: SAMN27578394). Metabolomic raw dataset with processed files and the entire details of used samples can be downloaded using the following link: https://figshare.com/s/5f84cf321e731a49ae06 (DOI: https://doi.org/10.6084/m9.figshare.19486883). 16S rRNA amplicon sequencing dataset with processed files and the entire details of used samples can be downloaded using the following link: https://figshare.com/s/077130437ca8ac314386 (DOI: https://doi.org/10.6084/m9.figshare.19483346).
- No new code was developed in this study. All scripts and metadata, together with GraphPad Prism files containing statistical analysis for alpha diversity, bacterial count, and taxonomy profile are on GitHub (https://yilmazbah.github.io/StomaMicrobiota).
- Any additional information required to reanalyze the data reported in this paper is available from the corresponding author, Bahtiyar Yilmaz (bahtiyar.yilmaz@dbmr.unibe.ch), upon request.

EXPERIMENTAL MODEL AND SUBJECT DETAILS

Study design

We included patients with original diagnoses of colorectal cancer (CRC), ulcerative colitis (UC), Crohn's disease (CD), and healthy individuals for three different sections of the study. The first part of the study consists of 13 CRC patients who were longitudinally sampled for luminal content and biopsies before and after stoma surgery. The second part of the study includes 79 CRC, 19CD, 16UC stoma patients, and 14 healthy subjects. Luminal (stoma) or fecal contents were used for microbiota profiling in these patients. In the third part of the study, luminal stoma contents from cured 6 CRC patients who had fasted overnight (at least 10h) were collected during the day every two hours to study the effect of feeding on ileal microbiota. The details of the samples are described in *Sample collection* section of method details.

Ethics statement

Licensed gastroenterologists collected biopsy and luminal samples and clinical data of patients. Stoma patients were anonymized and collected in EDC (electronic data capture) system (REDCap) activated for the trial after successfully passing formal quality controls. The Bern EDC system and the database are hosted by the Clinical Trial Unit of Bern University. The Bern Human Intestinal Community project for stable stoma samples and the Bandit project for longitudinal samples were approved by the Bern Cantonal Ethics Commission (Ref: KEK-BE: 251/14 and BASEC number (2021-01108); and KEK-BE:2017/00573, respectively) with signed informed consent was obtained from all participants.

METHOD DETAILS

Sample collection

In the first part of the study (Figures 1 and S1A–S1D), ileal and rectal samples from 13 subjects were collected directly before and at surgery, followed by sequential sampling from the same patient over the next 6-12 months Table S1. Samples were collected at 7-time points during the primary rectal cancer surgical treatment. Timepoint 0 (E0) is prior to surgery. Rectal biopsies and luminal contents were collected during the colonoscopies and at the time of surgeries. Timepoint 1 (E1) is the time of the surgical resection of rectum and the formation of the protective loop. During the formation of the protective loop ileostomy, a sample of the small bowel effluent and a 0.5x0.5 cm small bowel mucosa biopsy were collected. Time points 2-7 (E2-E7) are different time points starting from day 5-7 (postoperatively after resection of rectal cancer, before discharge) until 300 days (ileostomy closure): small bowel effluent from the afferent limb, swab specimen out of the efferent limb of the ileostomy and small bowel effluent from the afferent limb during closure surgery, rectal biopsies and luminal contents were collected into 2ml tubes. Samples were then stored at -80°C until DNA extraction.

In the second part of the study (Figures 2, S1E, S4D, S4E, and S5), the luminal contents were collected from either stoma or stoma bag from different intestinal locations of 79 patients who had recovered from surgery for distal colonic cancers (CRC) (38% ileostoma, 10% right-sided colonic stoma, and 52% left-sided colonic stoma) and 19 CD patients (47% ileostoma, 32% right-sided colonic stoma, and 31% left-sided colonic stoma) and 16 UC patients (100% ileostoma). Samples were divided into 3 tubes and later used for 16S amplicon sequencing, metabolomics, and total bacterial count (see Figure S1A and Table S3 for anatomical and clinical details). In addition, fecal samples were collected into OMNIgene•GUT tubes by 17 healthy donors and were stored at -80°C until DNA extraction. The fecal samples from healthy donors were not used for any metabolomics, or total bacteria count since the samples were collected into OMNIgene•GUT tubes which stabilized the microbial DNA. Fecal samples from additional two healthy controls were collected longitudinally every 2 weeks into OMNIgene•GUT tubes and were then stored at -80°C.

In the last part of the study (Figures 3 and 4; Figures S2 , S3, S4A–S4C, S6, and S7), we collected serial samples from ileal stomas in cured 6 CRC patients who had fasted overnight (at least 10h) before and after they had eaten a standardized breakfast provided by hospital catering. The breakfast contained bread, cheese, butter, olive, yogurt, jam, and coffee with milk, while lunch contained chicken breast or beef strips together with pasta or french fries, salad, mineral water, and coffee with milk. Early in the morning, at time point 0 (t=0h) first content samples were collected into 2ml Eppendorf tubes from the ileum before they had eaten breakfast (breakfast time), and samples were then collected at 2 (t=2h), 4 (t=4h; lunchtime), 6, 8, 10 and 48h (t=6-48h). Luminal samples were divided into two tubes and later were used for shotgun metagenomic sequencing and metabolomics. Contents were then centrifuged at 4°C and were snap-frozen in liquid nitrogen. Samples were then stored at -80°C until DNA extraction.

We then recruited four additional patients who also fasted overnight, and ileal content samples were collected from these patients at three different time points before (t=0h) and after they had eaten a standardized breakfast (t=2h and t=4h) (Figure 3D) and stored at -80°C until the DNA extraction.

DNA extraction from human intestinal biopsies and luminal contents

DNA was extracted from luminal contents, small bowel effluents, and endoscopic biopsies that were initially collected into 2ml microfuge tubes using AllPrep DNA/RNA Mini Kit (QIAGEN) or QIAamp DNA stool kit (Qiagen) according to the manufacturer's instructions. Briefly, 700 μl of Buffer RLT Plus 2-mercaptoethanol and a metal bead were added to each tube containing biopsies. Biopsy samples were then homogenized with the Retsch Tissue Lyser (QIAGEN) at 30Hz for 3 min, followed by 3 min centrifugation at 13000g (Eppendorf). Supernatants were transferred into the AllPrep DNA Mini spin column and centrifuged at 10000g for 30 sec. DNA within spin columns was washed using 500μl of Buffer AW1 and Buffer AW2 afterward (Yilmaz et al., 2019). Alternatively, luminal DNA extraction was QIAamp DNA stool kit (Qiagen) according to the modified manufacturer's instructions (Yilmaz et al., 2021). Briefly, 100 mg luminal contents were homogenized in 500μl Buffer ASL buffer by bead-beating step as described above and followed with 95°C heat-based lysis steps. This step was modified from the manufacturer's protocol. After repeating bead beating and heating steps twice, samples were incubated with 200μl Lysis Buffer (20mg/ml lysozyme (added after autoclave - Sigma 62970-5G-F); 20mM TrisHCl, pH 8.0; 2mM EDTA; 1.2% Triton) for 30 min. This step allowed us to increase the DNA yield for difficult to lyse gut microbiota components. Next, 500μl Buffer ASL was added, and the manufacturer's protocol was continued for downstream processes. In both extractions, DNA samples were eluted with 30μl DNase/RNase free water, and the concentration/purity of the extracted DNA samples was assessed by NanoDrop® (Thermo Scientific). Samples were then stored at -20°C until amplicon PCR or shotgun metagenomic sequencing.

16S amplicon sequencing using IonTorrent PGM platform

The V5/V6 region of 16S rRNA genes was amplified with Invitrogen™ Platinum™ *Taq* DNA polymerase from 200-1000ng of DNA. The expected product length was ~350 bp. The bacteria-specific primers (forward 5'-CCATCTCATCCCTGCGTGTCTCCGACTCAGC-barcode-ATTAGATACCCYGGTAGTCC3' and reverse 5'-CCTCTCTATGGGCAGTCGGTGATACGAGCTGACGACARCCATG-3') were used (Sundquist et al., 2007).

PCR conditions consisted of an initial 5 min at 94°C denaturation step, followed by 35 cycles of 1 min denaturation at 94°C, 20sec annealing cycle at 46°C, and 30sec extension cycle at 72°C, with a final extension for 7 min at 72°C. PCR products run on 1% gel for 2 hours and amplicons were purified using Gel Extraction Kit (Qiagen). The amplicon concentration was determined with Qubit 3.0 Fluorometer (ThermoFisher). 26pM of each sample were pooled into a library tube and sequencing was then carried out using the Ion PGM™ Sequencing 400 Kit and Ion 316™ Chip V2 within the IonPGM™ System (Thermo Fisher) (Yilmaz et al., 2019).

Raw sequences were first loaded into the QIIME 1.9.1 pipeline, as described (Caporaso et al., 2010) on the UBELIX Linux cluster of the University of Bern. Only samples with more than 5000 high-quality reads were used for further analysis using R packages. Operational taxonomic units were picked using UCLUST with a 97% sequence identity threshold as a default option implemented in QIIME, and followed by taxonomy assignment using the latest SILVA rRNA database (https://www.arb-silva.de) (Pruesse et al., 2007). OTUs that were not present in at least 30% of our samples or with a low abundance (<0.0001% of the total counts) were filtered out from the downstream analysis. In combination with the detailed clinical patient metadata (diagnosis, age, BMI, gender, location of stoma, treatment, diet, smoking status, etc.) downstream analysis and data visualization were performed in the R statistical programming environment package *phyloseq* (McMurdie and Holmes, 2013). Since the general consensus is not to rarefy the data, this was not carried out on the dataset for the downstream analysis (McMurdie and Holmes, 2014). The statistical differences in α-diversity (Shannon index) were calculated either with a non-parametric Kruskal-Wallis test or Mann-Whitney U test for group comparisons or linear mixed models for longitudinal samples where we assessed the distribution of variation [*lmer(Diversity ~ TimePoint + Age + BMI + Antibiotic + Gender + (1|PatientID) + (1|SmokingStatus), data = diversitydata)*].

To evaluate differences in community composition (β-diversity), Bray-Curtis genus-level community dissimilarity distances were calculated and plotted. For a Bray-Curtis Dissimilarity measure in beta diversity analysis, we used the relative abundance data of each taxon in every sample. Differences in beta-diversity between the groups were assessed (PERMANOVA) with pairwise comparison (Benjamini-Hochberg false discovery rate correction) using *pairwiseAdonis* R package. (Callahan et al., 2016; McMurdie and Holmes, 2013). Multivariate homogeneity of group dispersion was to calculate the average distance of the groups and to test if the dispersion of any group was significantly different from the others using *betadisper* command from *vegan* R package with the implementation of M. Anderson's PERMDISP2. MaAsLin2 with implemented multiple testing (Benjamini-Hochberg false discovery rate correction; a false discovery rate [FDR], q-value) was used to find associations between clinical metadata and microbial community abundance (Mallick et al., 2021; Morgan et al., 2012). Taxa present in at least 10% of the samples and minimum 0.00001% of total abundance were set as the cut-off values for further analysis. The differences between groups were tested at phylum, family, and genus levels *with analysis method = LM* after converting the abundance table (feature table) into relative abundance and logarithmic transformation. Random and fixed effects, as stated for alpha diversity analysis of longitudinal samples, were also included in MaAsLin2. The following commands were the representative command line for MaAsLin2 analysis when the taxonomy data was read count:

fit_data <- Maaslin2 (input_data_bacteria, input_metadata, 'AnalysisName, transform = "LOG", min_abundance=0.000001, normalization="CSS", method="LM", max_significance=0.2, min_prevalence=0.1, fixed_effects = c('Diagnosis', 'Sample_Style', 'BMI', 'Age', 'Gender'), random_effects = c('Smoking_Status', 'Antibiotics_3months', PatientID), standardize = FALSE)

In contrast, when the taxonomy data is the relative abundance, the centered log ratios normalization with log transformation was used in MaAsLin2.

After the correction for a false discovery rate, the adj-p value <0.05 was considered significant. Differences of p<0.05 were considered significant in some of the statistical analyses. Statistically significant differences are shown with asterisks as follows: *; adj-p < 0.05, **; adj-p < 0.01, ***; adj-p < 0.001 and ****; adj-p < 0.0001. Notable near-significant differences (0.05<p and 0.05< adj-p-value <0.2) were also highlighted in some of the figures and following asterisks were also used: *; p < 0.05, **; p < 0.01, and ***; adj-p < 0.001. Non-significant data is shown with "n.s.". All the relevant codes for running the MaAsLin2 are available on Dr. Huttenhower's group webpage (https://huttenhower.sph.harvard.edu). Plots were generated with ggplot2 using a *phyloseq* object or GraphPad Prism v9.

Determination of the biomass

The weighed stoma luminal contents collected from 4 patients fasted overnight (t=0h), and after feeding t=2h and t=4h were suspended in 1ml PBS, and fiber-filtered (100μm) suspensions were diluted to OD_{700}=~0.8, stained with SYTO9 (5μM), and acquired at a Beckman Coulter MoFlo® ASTRIOS™ with known concentrations of spiked-in Fluoresbrite BB Carboxylate microsphere beads of various sizes (0.5 μm, 1 μm, 2 μm). Bacteria were identified with SYTO9+. The bacterial concentration was calculated as described elsewhere (Yilmaz et al., 2021). Differences between time points were tested with paired non-parametric tests corrected for multiple comparisons by controlling the FDR using the two-stage linear step-up method of the Benjamini, Krieger, and Yekutieli.

Metabolomics

For extraction of metabolites, 4X volume of cold MeOH (final conc. 80%) was added to the supernatant part of luminal content samples and incubated for 1h at -25°C. Samples were then centrifuged for 3 min at 20 000g at room temperature. The supernatant was collected and sealed in 96-well plates. A 6550 Agilent Q-TOF mass spectrometer was used to quantify relative metabolite ion abundance in 1:10 diluted samples by non-targeted flow injection analysis as described previously (Uchimura et al., 2018). Profile spectra with high mass accuracy were recorded from 50 to 1000 m/z in negative ionization mode. Ions were annotated based on accurate mass comparison using 3mDa mass tolerance against unique molecular weights of compounds present in the Human Metabolome Database (Wishart et al., 2013). The adj-p-value < 0.05 and absolute fold change (log_2) > 2 were calculated from quantile-normalized ion counts using MatLab R2020b and used as a cut-off parameter for visualization. One-way ANOVA with Tukey's HSD test was used to test the significance of metabolite differences between intestinal locations (Figures S4D and S4E).

Quantile-normalized ion counts were z-score transformed for k-means clustering, and the appropriate number of 10 clusters was determined based on the mean sum of point to centroid distances (Figure S4A).

Library preparation and sequencing for metagenomics

Bacterial DNA libraries were prepared according to the Nextera DNA Library Prep (Illumina) and sequenced on NovaSeq 6000 (Illumina) in paired-end mode to produce 2 x 150bp reads. The metaWRAP-Read_qc module was then used to 1) filter out the human genome–contaminated reads by aligning reads to the human reference genome, hg38 (UCSC) and 2) remove adaptor sequences and low-quality reads, and produce quality reports for each of the sequenced samples, prior to the microbial abundance estimation (Uritskiy et al., 2018). This module includes the FASTQC (Andrews, 2015) and the BMTagger pipelines (Rotmistrovsky and Agarwala, 2011). Afterward, bacterial strain level were assessed using the Metagenomic Intra-Species Diversity Analysis System (MIDAS) with the sample and site depth > 5 (Nayfach et al., 2016).

The taxonomy assessments of viral strains together with plant and fungi one was using the Kraken2 pipeline with a custom RefSeq database following the developer's guideline and a Kraken report was generated in https://github.com/DerrickWood/kraken2/blob/master/docs/MANUAL.markdown#custom-databases (Wood et al., 2019; Wood and Salzberg, 2014). We used *kraken2-build –download-taxonomy –db CustomDB* to download in the CustomDB taxonomy folder i) taxonomy the accession number to taxon maps, as well as the ii) taxonomic name and iii) tree information from NCBI which only contains the complete genomes of archaea, bacteria, fungi, plants, protozoa, and virus. Afterwards, custom database containing all taxa except plants was built using kraken2-build command and plant taxonomy analysis was separately run with only plant and human database together.

The following command line was representative for taxonomy classifications using Kraken2:

- *kraken2 –use-names –db /home/ubelix/dbmr/terziev/CustomDB –fastq-input –report-zero-counts –confidence 0.2 –threads 24 –minimum-base-quality 0 –paired –gzip-compressed {input_1.fastq.gz} {input_2.fastq.gz} – output {output.reads} –report {output.report} > input.kraken*

Afterwards, Bracken (Bayesian Re-estimation of Abundance with KrakEN) (Lu et al., 2017) was used to refine the read counts at lower levels of the taxonomy, and re-estimate at the levels of species, genus, and family using Kraken2 output. We used the default command line as shown here: https://genomics.sschmeier.com/ngs-taxonomic-investigation/index.html#bracken.

The inStrain pipeline

This pipeline was used for the analysis of population genome comparisons, reporting of gene coverage and breadth, SNV calling with gene localization and synonymous/nonsynonymous identification, nucleotide diversity, and dN/dS ratio for feeding experiments. Full documentation available online at https://instrain.readthedocs.io was followed and personal communication with Dr. Matthew R. Olm, one of the developers of this pipeline, to validate the output (Olm et al., 2021). For each genome, sample-specific base-pair coverage and the number of bases of the genome covered by at least one read were calculated from sequencing data obtained after *metaWRAP-Read_qc* module. We ran the following commands to get the SNVs and dN/dS profile for each sample:

- ***inStrain profile*** *SF${SLURM_ARRAY_TASK_ID}.sam UHGGv1/UHGG_reps.fasta -p 24 -g UHGGv1/UHGG_reps.genes.fna -o StomaMetagenomics/Instrain/SF${SLURM_ARRAY_TASK_ID}.IS -p 24 -g UHGGv1/UHGG_reps.genes.fna -s UHGGv1/UHGG_reps.stb –database_mode.*
- ***inStrain compare*** *-i Instrain/SF${SLURM_ARRAY_TASK_ID}.IS -s UHGGv1/UHGG_reps.stb -p 24 -o StomaMetagenomics/Instrain/IS.COMPARE –database_mode*

More than 10X of a cumulative depth of coverage across all samples was set as a cut-off for a genome to be considered in downstream analysis. Additionally, at least 80% breadth of the genome coverage (the criterion for the species to be considered present) from at least one sample was used to remove species that are not present in feeding cohort samples. We included the SNPs that have the value higher than zero in over 80% of the samples. We also filtered out the SNPs that had a value of 1 in more than 80% samples.

Strain-level comparisons were performed between subspecies detected in multiple samples from the same patients over time-series sampling in Figures 3 and 4. For the strain comparisons within-patients or between-patients, all strains detected in multiple individual samples from a patient were compared using 'inStrain compare'. A distance matrix was then created for each subspecies based on population average nucleotide diversity (popANI) values, and this matrix was used to cluster strains into a number of

individual strains using 'average' hierarchical clustering with a threshold of 99.999% ANI with the *scipy* cluster package. Strains with PopANI > 99.999% were named identical ''shared'' strains, and strains detected with PopANI=81% - 96% are named non-identical ''non-shared'' strains. Lastly, the ''pairwise approach'' identified strains that shared >99.999% popANI across consecutive sampling. We chose the cutoff of 99.999% popANI for persistence following the calculation performed before describing the expected rate of *in situ* bacterial evolution in the human gut (~0.9 single-nucleotide polymorphisms (SNPs)/genome/year) (Zhao et al., 2019).

The nucleotide diversity (π) of each position is calculated using the following formula $\pi = 1 - [(\text{number of 'A' bases/total bases})2 + (\text{number of 'C' bases/total bases})2 + (\text{number of 'T' bases/total bases})2 + (\text{number of 'G' bases/ total bases})2]$ as implemented in inStrain pipeline and the obtained values obtained here were then used to calculate the average nucleotide diversity for each genome.

All software was run parallelized on a high-performance computing (HPC-UBELIX) cluster at the University of Bern.

Variant annotation

Variant annotation for *E. coli* and *K. pneumonia* was also done using modified inStrain on output files (Yilmaz et al., 2021). Pilon pipeline was run to identify larger structural variants and putatively problematic regions in the assemblies (Walker et al., 2014). Then, overlapping intervals were collapsed within samples and then merged to produce one summary table per species. LoFreq pipeline was used for variant calling (Wilm et al., 2012). The variants detected in a first round were used as known sites for base quality score recalibration using theGenome Analysis Toolkit (GATK) (McKenna et al., 2010). The output was reformatted usinga custom script and merged across samples withvcftoolsv. 0.1.15 to produce one variant call file per species (Danecek et al., 2011). Variants were annotated with *SnpEff* v. 4.3T (Cingolani et al., 2012) using databases built from *gff* files with annotations from RAST (Aziz et al., 2008). *VariantAnnotator* from GATK v.3.7 was used to simplify the annotations, retaining only the one with the biggest effect. A custom script was used to generate a final table with all positions where an alternative allele was detected in at least one of the samples. Positions with more than one alternative allele were removed. The full variant calling workflow was implemented as an automated pipeline in the *snakemake* 5.3.0 (Köster and Rahmann, 2012).

Structural variation identification and annotation

The highly variable genomic segments within bacterial genomes that can be potentially absent and present with variable abundance were detected using SGVFinder, a tool devised and described by David Zeevi and Eran Segal to detect two types of SV – deletion SVs (dSVs) and variable SVs (vSVs) – from metagenomic data. (Zeevi et al., 2019). We also followed the https://github.com/GRONINGEN-MICROBIOME-CENTRE/Groningen-Microbiome/tree/master/Scripts/SV_pipeline for installation of the tool in which stated for the corrections in of *SGVFinder.py* and *SGVF_cmd.py*. The pipeline considers 1) the variable SV if the deletion percentage of the genomic segment across the population is < 25%, 2) the deletion SV if the deletion percentage of the genomic segment across the population is > 25% and < 75% and 3) exclusion of region if the percentage of a deletion region is > 75. We then used the reference database provided by *SGVFinder* that is based on the *proGenomes* to annotate the genes (http://progenomes1.embl.de) (Mende et al., 2017).

QUANTIFICATION AND STATISTICAL ANALYSIS

Unless otherwise stated in the individual method sections above, all statistical analyses were performed using R version 3.6.1 (2019-07-05) or Prism 9 (GraphPad Software, San Diego, CA).Differences between the two groups were evaluated using Mann–Whitney U test (non-parametric) and more than 3 groups were tested using one-way ANOVA (parametric), followed by Tukey's honest significant difference test or two-stage step-up method of Benjamini, Krieger, and Yekutieli, as a post hoc test. Meanwhile, alpha diversity of effluent and mucosa samples over time after surgery from different patients and alpha diversity changes after fast-feeding cycles were tested with linear mixed models, as described above. Microbial changes were tested using multivariate analysis by linear models (MaAsLin2) R package (Mallick et al., 2021; Morgan et al., 2012) as detailed in *Analysis of taxa changes*. Adonis (PERMANOVA) for beta diversity with pairwise comparison (Benjamini-Hochberg false discovery rate correction) using pairwiseAdonis R package to confirm the strength and statistical significance of groups in the same distance metrics with the phyloseq pipeline in R (Callahan et al., 2016; McMurdie and Holmes, 2013). Differences of $p < 0.05$ or adj-$p < 0.05$ were considered significant in all statistical analyses. Statistically significant differences are shown with asterisks as follows: *; adj-$p < 0.05$, **; adj-$p < 0.01$, ***; adj-$p < 0.001$ and ****; adj-$p < 0.0001$. Notable near-significant differences ($0.05<p$ and $0.05<$ adj-p-value <0.2) were also highlighted in some of the figures and following asterisks were also used: *; $p < 0.05$, **; $p < 0.01$, and ***; adj-$p < 0.001$.